Chapter 1

ATOMIC-LEVEL PROPERTIES OF THERMAL BARRIER COATINGS : CHARACTERIZATION OF METAL-CERAMIC INTERFRACES

Asbjorn Christensen, Emily A. Asche and Emily A. Carter

Department of Chemistry and Biochemistry
Box 951569
University of California, Los Angeles
Los Angeles, California 90095-1569, USA

1. INTRODUCTION AND CHAPTER OVERVIEW

This chapter considers basic research related to the extreme environment of an aircraft engine and the use of Thermal Barrier Coatings (TBC's) to ameliorate the effects of extreme temperature cycling on metal engine components. The failure of these TBC's is a serious technological problem; one that, if solved, should greatly increase the fuel efficiency and operating lifetimes of airplane engines. These TBC's are comprised of ceramics, with favorably low thermal conductivity, deposited on the engine metals. Accordingly, we are concerned with the characterization of Metal-Ceramic (M/C) interfaces at a fundamental level. In this chapter, we attempt to provide an overview of experimental techniques for characterizing M/C interfaces. However, since we are theorists, much of the review is focused on providing a detailed, critical analysis of theoretical methods in use today to study such systems. We also give examples from our own modeling at the atomic level that has yielded some insights into the interfacial behavior of TBC's.

Let us outline the problem caused by the extreme combustion environment. The ideal engine would operate at very high temperatures without failure in order to have the highest fuel efficiency. Typically, the combustion gas is held at temperatures above 1370 ^{o}C, while the metal superalloys that constitute the engine components have melting points ranging from 1230-1315 ^{o}C! This makes it imperative to either cool the metal components (e.g., by drilling holes and flowing cool air) or to provide thermal protection from

the combustion gas.[1] Ideas for optimizing the cooling techniques and engine metal alloy compositions reached a point of diminishing returns at least 10 years ago.[2] Hence, engineers looked to ceramic materials as a means of providing a thermal barrier coating that will: (i) extend the life of gas turbine components, (ii) reduce cooling requirements (thereby decreasing fuel consumption), or (iii) allow for an increase in gas inlet tempratures (thereby increasing thrust).[3]

Ceramics are thermal insulators that can provide the thermal barrier desired. The challenge of working with such ceramics is that typically they have completely different thermochemical properties from the material to which they are expected to adhere, namely a metallic alloy. As a result, the usual thermal cycling that such M-C interfaces undergo tends to stress these interfaces to the point of fracture and spallation (chipping-off).[1] It has been suggested that research is needed to try to connect these macroscopic phenomena to microscopic properties, in order to make progress in understanding how to design the best M/C junction.[4,5] In particular, the exact nature of the interface at the atomic level is poorly characterized; the exact mechanisms have yet to be identified by which the interface is formed, stressed, fractured, and spalled. Furthermore, it remains unclear what roles oxidation and temperature play in stabilizing or destabilizing the interface. Gaining an atomic-level understanding of these mechanisms, should help elucidate ways to optimize the M/C couple: simultaneously maximizing thermal insulation and minimizing spallation.

This chapter initially explores the TBC from an experimental point of view. In Section 2 of this chapter, we present a detailed description of the TBC structure and composition. We explore the typical chemical make-up of a TBC, the formation of the thermally grown oxide, and the physical methods used in TBC fabrication. Section 3 lists a number of the experimental techniques used to characterize functional TBC's and explains some experimental characterization of ideal interfaces. Section 4 investigates the problem of TBC spallation. This includes identifying likely perpetrators of spallation, describing proposed spallation mechanisms, looking at some features that complicate spallation studies, and expounding on the issue of adhesion. We also mention some of the techniques used for measuring stress, fracture, and spallation at the end of this section. After looking at TBC's from an experimental standpoint, we turn our discussion to present applicable theory. We describe atomistic modeling approaches in Section 6 and how those can be applied to M/C interfaces. This includes exploring the use of cluster and slab models, the idea of interface stoichiometry, and the problem of lattice misfit. We then consider the available *ab initio* techniques for modeling M/C interfaces. This is broken down to more specific meth-

ods including quantum chemical approaches, density functional theory, the approximation of the Harris functional, and tight binding schemes. We also present results obtained from a number of density functional theory studies, including our own, as well as tight binding predictions. Section 7 and 8 review theory designed to handle larger systems than are computationally feasible with the *ab initio* techniques. Finally, we offer brief conclusions that attempt to look to the future for ways of enhancing understanding of and optimization of thermal barrier coatings.

2. CREATING A TBC SYSTEM

2.1. Commonly Used Materials

When creating a TBC, generally a top coat and a bond coat layer must be deposited. The top coat serves as the insulator and the bond coat mediates contact between the top coat and metal alloy substrate. The nickel-based "superalloy" substrate is a real pot pourri of elements, consisting of Ni, Co, Cr, Mo, Al, Ta, Ti, C, Zr, and B (where the non-Ni elements are present at the few to hundredths of a weight percent level.)[6] Yttria-Stabilized Zirconia (YSZ) is a favored top coat material. Pure zirconia has relatively high strength, wear resistance, and fracture toughness. Likewise, it exhibits an extremely low thermal conductivity. In fact, excluding Pyrex glass, the thermal conductivity of zirconia is lower than any other engineering ceramic by over an order of magnitude.[6] In practical terms, this property allows even a thin zirconia film (less than one millimeter thickness) to potentially reduce the temperature of the underlying alloy several hundred degrees Celsius.[7] Furthermore, the linear thermal expansion coefficient and elastic modulus of zirconia (especially the tetragonal phase) are well-matched to several popular nickel-based superalloys, compared to possible alternative ceramics. These properties are essential to coating survival during thermal cycling.[7–9] Unfortunately, zirconia also exhibits polymorphism as a function of temperature, primarily between the monoclinic, tetragonal, and cubic phases. Although the polymorphism can be exploited to inhibit crack propagation via volume changes that occur upon transformation,[7,10,11] unregulated polymorphism can be detrimental to TBC functionality. As a result, other cubic oxides are added to control or eliminate polymorphism. Partial stabilization of the tetragonal phase across the relevant temperature range affords some phase control yet preserves the valuable inhibition of stress-induced micro-crack propagation. Greater than 8.5 mole percent Y_2O_3 dopant produces fully-stabilized cubic zirconia while a 2-8.5 percent Y_2O_3 concentration creates a partially stabilized (tetragonal) form;[12] similarly, adding CeO_2, CaO, or MgO can generate stabilized zirconia.[13–16] Conversely, using TiO_2 as the

stabilizing oxide is less effective than the other oxides studied.[17,18] However, TiO_2 added to Y_2O_3 or CeO_2 stabilized ZrO_2 has been shown to produce zirconia polycrystals with favorable properties.[19,20] Although a percentage of the partially stabilized ZrO_2 tends to remain in the monoclinic phase throughout thermal cycling, the initially formed cubic phase converts to tetragonal after thermal treatment in air.[21,22] Despite the favorable properties of a YSZ top coat, the difference in thermomechanical properties between a YSZ top coat and a metal-alloy substrate is enough to require the introduction of an intermediate layer. This bond coat is important for adhesion and grading the thermal expansion mismatch between the top coat and substrate. A typical bond coat contains nickel, chromium, aluminum, and yttrium, with nickel as the primary element for nickel-alloy substrate applications. With other alloys, it is sometimes desirable to use iron or cobalt in place of the nickel in the bond coat.[23,24]

2.2. Formation of the Thermally Grown Oxide

A third layer present in a TBC is the Thermally Grown Oxide (TGO). Bond coat oxidation can reduce TBC adhesion to the substrate. In most cases, the oxidation products begin to form even prior to top coat deposition. It is standard practice, in zirconia film creation chambers, to supply oxygen to ensure stoichiometry of the zirconia layer. Moreover, the bond coat continues to be oxidized once the zirconia layer is in place, since zirconia readily conducts oxygen ions at high temperature.[25] Accordingly, the TGO layer between the bond coat and top coat thickens with thermal cycling. Although this layer is generally thin compared to the TBC layer, it can lead to large stresses in the system due to significant thermal expansion mismatch of the TGO and bond coat.

The growth of the TGO falls into two primary regimes. Fast initial growth of non-protective oxides is followed by continuous protective scale growth, largely controlled by diffusion. The primary protective scale formed with bond coat oxidation is alumina, Al_2O_3. For a bond coat composed of NiCrAlY, the oxidation also produces $Ni(Cr,Al)_2O_4$ spinels, Y_2O_3, NiO, $AlYO_3$, and $Al_5Y_3O_{12}$ bands oriented perpendicular to the bond coat.[23] In the initial oxidation stages, X-ray diffraction of a FeCrAlY bond coat indicate that both $FeCr_2O_4$ and Cr_2O_3 form in that system.[24]

Oxide scale studies are complicated further by the coexistence of various oxide phases. For instance, at early times, both Θ-alumina, a transient phase formed when γ-alumina is heated, and α-alumina are present. Amorphous alumina transforms through a series of metastable phases until the more stable α-alumina dominates at long oxidation times.[26] Although thicknesses of the layers vary, some fairly typical values are 250-500 μm for the top

coat, 100-150 μm for the bond coat (this varies since some bond coats are designed for surface roughness and with several gradation layers), and about an order of magnitude less than these for the thermally grown oxide.[23] Fig. 1 displays a schematic cross-section of a TBC.

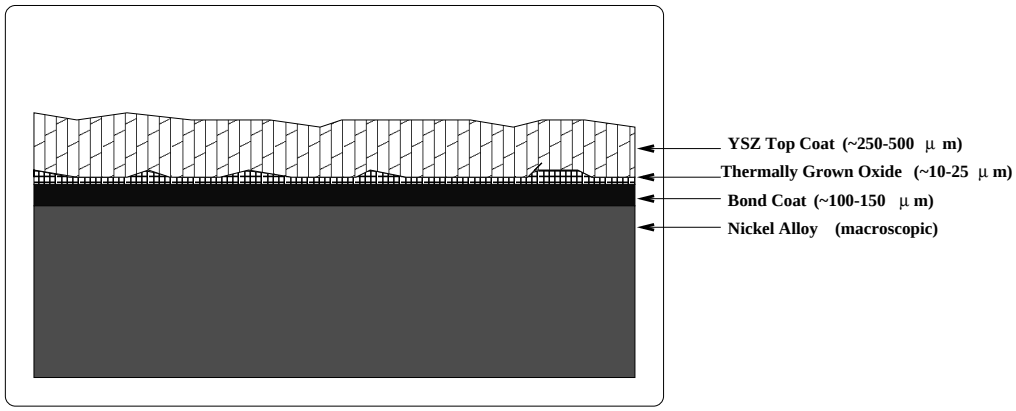

Figure 1 Cross-section of a TBC (not pictured to scale)

2.3. Depositing the TBC and Bond Coat

Several methods effectively apply thin coatings to substrates. One process commonly employed for TBC fabrication is thermal plasma spraying. For this technique, the bond coat is deposited with low pressure plasma spraying and the ZrO_2 top coat is then created using atmospheric plasma spraying.[27] A potential problem with this method is coating fracture due to weak interlamellar adhesion, resulting from discontinuities within the solidifying process.[28] Accordingly, plasma sprayed coatings tend to fail within the TBC itself. Alternatively, electron-beam physical-vapor deposition can be used for TBC fabrication. One drawback of this method is possible spallation, via separation at the bond coat interface during cooling.[26] Nevertheless, successful coatings of this type possess columnar micro-structure, supplying some of the stress compliance required by the TBC. Furthermore, this method is suited for creating a graded Al_2O_3-ZrO_2 layer. It is hoped that a gradual transition from the bond coat oxide to the top coat would improve the life of the TBC;[29] however, more work is needed to understand the practical effectiveness of such a layer.[30] Sputter deposition is another useful means for producing thin coatings.[31,32] Each deposition method has its own set of pros and cons, hence this variety in fabrication techniques continues.

3. CHARACTERIZING THE TBC

3.1. Characterization Techniques

Advanced characterization methods are required to gain a microscopic-level understanding of TBC's. High-Resolution Transmission Electron Microscopy (HRTEM) and Scanning Electron Microscopy (SEM) are frequently used to explore the structure of the coating surface and the metal-oxide interface.[22,33,34] SEM also provides a qualitative thickness measure of oxide growth. The coating's porosity can be measured by image analysis techniques and mercury porosimetry. Use of the latter can pose difficulties since large pores are filled with mercury prior to applying pressure. Conversely, image analysis is ineffective for measuring very small pores and microcracks.[35] X-ray diffraction provides a means to determine the oxide species and phases.[22] Likewise, field-emission SEM and energy dispersive spectroscopy aid in characterizing oxidation products.[23] Microindentation tests determine the elastic modulus of the prepared coatings; however, due to inherent inhomogeneity in the coatings, results from this method must be appropriately averaged.[35] Thermal conductivity measures have been provided by laser flash methods that measure diffusivity and specific heat measurements from differential scanning calorimetry.[36,37] Alternatively, diffusivity values can be obtained with a multiproperty apparatus that measures temperature gradients, sample geometry, and heat flux.[38] The single-wavelength pyrometer method gathers spectral effective emissivities. Although thermocouples could also be used, the single-wavelength pyrometer technique has the superior attributes of not requiring surface contact during temperature measurements, immunity to electromagnetic interference from the surroundings, and no system perturbation during measurements.[39] The use of Auger Electron Spectroscopy (AES), X-ray photoelectron spectroscopy (XPS), and Auger parameter (α') analysis provide means to explore the nickel-alumina interface formation. Furthermore, these techniques are suited for determining ionicity and growth mechanisms at metal-oxide interfaces.[40]

3.2. Characterization of Ideal Interfaces

At high temperatures, interdiffusion leads to the formation of new phases at the M/C interface.[4] For example, Qin and Derby[41] used optical and electron microscopy to characterize the strength of Ni/ZrO_2 and Ni/NiO/ZrO_2 interfaces. They found that the strongest interfaces were formed by annealing Ni/ZrO_2 in air, which allowed a thin layer of NiO to form that helped adhesion to the ceramic. Qin and Derby also studied the formation of an interface between ZrO_2 and a Ni(Cr) alloy, where a mixed oxide with a spinel structure was formed at the interface.[42] The reaction at the interface

appeared to be accompanied by local melting after interdiffusion, although it is not clear which elements were actually diffusing. Wagner *et al.*[43] examined charge flow in a Ni|ZrO_2|Zr cell and showed that at 1273 K with no applied voltage, oxygen ions move from the Ni to the Zr electrode, forming Ni_5Zr and Ni_7Zr_2 at the Ni electrode while reducing ZrO_2 to Zr. At the Zr electrode, monoclinic ZrO_2 forms. Thus, oxygen ion diffusion appears to be an important process by which adhesion takes place.

As mentioned earlier, Al_2O_3 (TGO) also forms at the TBC-bond coat-superalloy junction. Trumble and Rühle[44] showed by Transmission Electron Microscopy (TEM) that at 1390 ° C, pure Ni does not form a spinel ($NiAl_2O_4$) at the interface between Ni and Al_2O_3. However, even 0.07 percent oxygen in the Ni will induce formation of a thin spinel layer at the interface (with no NiO intermediate required), where the kinetics appear to be controlled by oxygen diffusion. Shear strength measurements by Loh *et al.*[45] determined that, under conditions where the spinel $NiAl_2O_4$ is formed, fracture occurs along the spinel-Ni interface. It is still controversial as to whether formation of the spinel compound at these interfaces actually helps or hinders adhesion. Zhong and Ohuchi,[46] using X-ray photoelectron spectroscopy, and later Brydson *et al.*,[5] using spatially resolved transmission Electron Energy Loss Spectroscopy (EELS) and High Resolution Electron Microscopy (HREM), determined that the interface between Ni and Al_2O_3 forms direct Ni-Al bonds under reducing conditions at high temperatures. They presented evidence for a Ni_3Al phase at the interface, which they suggested was formed by Al diffusion into the Ni, and that this phase provides a driving force for the formation of Ni-Al bonds rather than Ni-O bonds. They suggested that formation of any spinel phase containing Ni-O bonds needs to be minimized because the spinel is brittle, an exactly opposite conclusion to that reached by Qin and Derby for the Ni-ZrO_2 interface.

In addition to M/C interactions, characterization of ZrO_2-Al_2O_3 is interesting as well, because of the Al_2O_3 that forms between the bond coat and the TBC. Aita and coworkers have grown and characterized with HREM nanolaminate films that alternate between polycrystalline ZrO_2 and Al_2O_3 layers. They have shown that ZrO_2 grows with the close-packed tetragonal(111) or monoclinic($11\bar{1}$) surfaces parallel to the substrate.[47] Interestingly, we recently calculated those surfaces to be the most stable for each of these two phases.[48] They also observed that the amount of t-ZrO_2 increases with decreasing ZrO_2 film thickness and that the crystallites grow in this tetragonal phase up to a critical thickness of about 6.0 nm, at which point additional ZrO_2 converts the crystallite into the monoclinic phase.[49] In other work, they showed that the stress-induced transformation of tetragonal to monoclinic zirconia is limited to nanometer-scale regions in these nanolam-

inates.[50] In Section 6.2.2.2, we discuss our own theoretical rationalization of these observations. The role of alumina seems merely to confine the size of ZrO_2 crystallites formed. Our own calculations on ZrO_2-Al_2O_3 (discussed in Section 6.2.2.2) are consistent with these observations.

4. TBC FAILURE

Differences in crystal structure, size, and thermal expansion coefficients between the top coat, bond coat, and substrate introduce strain into the TBC. The thermal expansion coefficient of the top coat is generally lower than that of the bond coat or the alloy substrate. As mentioned earlier, a properly designed bond coat serves as a graded thermal expansion layer to reduce the strain caused by thermal expansion mismatch. Unfortunately, thermal cycling in air enhances the mismatch and increases strain resulting from interfacial damage during oxidation.[24] With repeated cycling, this strain contributes to coating failure.

4.1. Likely Culprits

TBC failure involves a number of contributing factors. Obviously, the strains introduced with thermal cycling are a major area of concern. The buildup of the TGO, migration and segregation of the components, and phase transitions of the TGO and top coat may each contribute to the coating failure. Even the type of porosity in the coating, largely dependent on the coating procedure used, can affect the coating lifetime. A great deal of experimental work connected with TBC's exists in the literature. Ernst published an excellent review that covers many experiments performed before 1995.[4] Due to inherent complexities of TBC's, studies to elucidate the failure mechanisms generally concentrate on only certain aspects contributing to failure. The subtle relationships of all the factors are not fully understood; hence, further modeling and experiments are needed to gain a more thorough understanding of present weaknesses and possible future improvements.

4.2. Spallation Mechanisms

Spallation is the process by which the TBC peels off of the substrate; and naturally, after the coating has spalled, the continuous thermal protection layer no longer exists. Likewise, the spalled fragments can block gas flow, contaminate products, and permit corrosion. The failure of the TBC leading to spallation appears closely related to the damage process within the TGO layer. Unfortunately, due to the highly complex nature of the problem, there is limited understanding of how growth kinetics of the TGO and microcrack damage affect TBC lifetime. Three primary scenarios have been proposed

for the spallation mechanism.[51] The first of these states that a buckling effect can result from planar compressive stresses within the ceramic layer. It seems this is a plausible mechanism provided there exists an interfacial delamination crack, formed due to local conditions creating both out-of-plane and shear tensions. Recent microscopy data indicate spallation can proceed via this buckling mechanism when the delamination crack is at least sixteen times the TBC thickness.[51,52] However, for thick oxides, the buckling mode is not viable. Those systems may undergo a surface wedging effect.[53] This second model relies on the development of a through-thickness shear crack in the TBC due to compression.[54] Finally, a more recently proposed mechanism depends upon a void formation under the TBC and subsequent folding effects which may lead to cracking.[55] This effect is also known as "wrinkling" or "rumpling." Naturally, in addition to voids formed through thermal cycling, the pore-types initially created in the TBC may influence the eventual spallation mode. Although each model appears plausible in its description of the final spallation effect, an understanding that would elucidate dynamic evolution conditions leading to spallation is desired. Fig. 2 displays schematic diagrams of the three spallation models.

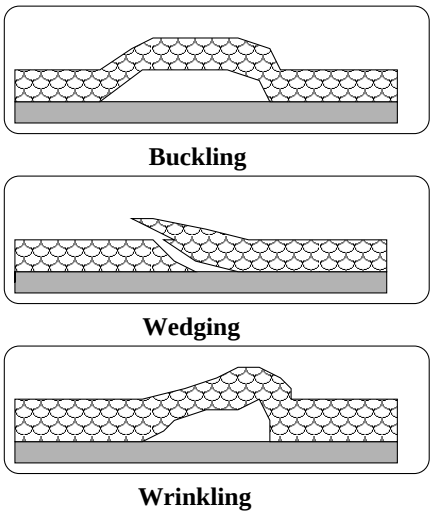

Figure 2 Spallation Mechanisms of the TBC

4.3. Complicating Features of Spallation

Although an understanding of spallation mechanisms is useful, it seems TBC and substrate delamination results from a highly complex relationship,

which includes bond coat oxidation, micro-crack evolution, and progressive buckling.[51] Fracture surfaces created by TBC spallation suggest that failure occurs in the TBC-bond coat interfacial region.[56] A piezospectroscopic study shows large failure regions may follow the oxide grain impressions in the bond coat, indicating failure where the TGO has grown into the bond coat grain boundaries.[26] Certain morphological instabilities of the oxide-bond coat interface may cause the fracture that joins the failure regions. These instabilities could result in local normal forces across the interface leading to interfacial fracture. A similar phenomenon occurs with spontaneous spallation after cooling a TBC to room temperature. Consequently, sub-critical crack growth may be hastened by environmental factors. Propensity for moisture to enhance such crack growth in metal-alumina interfaces further supports these ideas.[26,57,58] Using thermal plasma spraying for bond coat deposition may result in a layered bond coat with irregular thickness. Samples possessing this discontinuity in bond coat thickness failed after thermal treatment under an argon atmosphere, indicating that at least one factor in thermal spallation is increased residual stress on the YSZ after thermal treatment.[21] Thus, although the buildup of the TGO may play a large role in the eventual TBC failure, an overall spallation mechanism encompasses a variety of complicating features.[51]

4.4. Adhesion

Composition of the substrate and bond coat affects adhesion of alumina formed during bond coat oxidation. Of course, when the alumina spalls, the zirconia layer is not maintained; so the TBC fails. Migration, segregation, and stress generation are key areas of concern in the thermally grown oxide region. Migration of aluminum ions from bond coat to metal-alloy substrate occurs due to a concentration gradient. Likewise, migration from the substrate and bond coat into the thermally grown oxide region is also expected. Actually, it appears that limited yttrium ion migration to the alumina improves adhesion;[25] however, contaminants in the alumina generally lead to additional stresses, which decrease adhesion during thermal expansion.[59] The high temperature diffusion of bulk yttria ions to the YSZ surface destabilizes the top coat.[60,61] This permits zirconia phase transformation to monoclinic,[62] resulting in an undesirable volume expansion that may contribute to spallation. Furthermore, an SEM study shows bond coat aluminum can diffuse into the YSZ layer.[39] Previously, it has been suggested that both neutral and ionic aluminum diffusion into the YSZ layer induces spallation.[63] Accordingly, diffusion-controlled migration in the TBC may promote harmful phase transitions and enhance thermal stresses.

Although a concentration gradient allows migration via diffusion, the oxygen chemical potential gradient, arising during oxidation, supplies another driving force. Studies show that this chemical potential gradient penetrates the top coat, bond coat and into the metal substrate. It affects oxygen-reactive species in all these layers, including those initially in the form of stable oxides, nitrides, carbides and sulfides.[64–67]

Segregation to the metal-TGO interface also affects oxide adhesion. For instance, sulfur segregates to this interface, which can prove detrimental to TBC lifetime. The interfacial sulfur increases the thickness of the oxidation layer, decreases adhesion of the oxide layer to the metal, increases transformation of metastable alumina to the alpha phase, and enhances pore formation at the interface and within the oxide layer. Increased interfacial roughening and void formation results. The formation of voids is problematic since voids act as stress concentration sites within the oxidation layer.[65,68–72] De-sulfurization of the sample to less than 1 ppm may help prevent spallation.[73–76] However, it is possible that the presence of other species (such as Y and Zr) in the bond coat and substrate may supress the harmful effects of the sulfur and render de-sulfurization unnecessary.[25,65,77] Finally, scale stresses can result from isothermally generated growth stress during the oxide formation or from cooling stress due to thermal expansion mismatch during thermal cycling.[78]

4.5. Measures of Stress, Fracture and Spallation

In addition to experimental means for initially characterizing TBC systems, a number of techniques are useful for investigating stress, fracture, and spallation. Cr^{3+} piezospectroscopy is an optical method, sensitive to Cr^{3+} dopants in the alumina, that permits study of oxidation stresses through the TBC. Prior to this technique, non-destructive study of the oxide layer had proven difficult due to the physical location of the alumina. Fortunately, zirconia is fairly transparent at the frequencies of interest. As a result, this piezospectroscopic technique is able to detect stresses and some phase differences within the oxide layer.[79] Techniques for determining fracture energy include double cantilever-beam experiments,[80,81] four-point bending tests,[82–84] and wedge-loaded peel tests.[83] Furthermore, laser spallation provides a means to measure tensile strength of the metal-oxide interface.[85–87] Pulsed lasers, used as high shock generators, allow exploration of the spallation process through simulated high pressure loading.[88,89] A method based upon Thin Layer Activation (TLA) attempts to directly measure spallation. TLA relies on the creation of radionuclides in the surface layer after exposure to a high-energy beam of charged particles.[90,91] Loss of activated material due to spallation results in a decreased γ-activity signal. Furthermore, it

is possible to collect the spalled material, allowing mass quantification that provides an additional sensitive spallation measure.[92] Recently, effective measurements of amplitude and profile of laser generated stress pulses have been made using a Doppler velocity interferometer system for any reflector. An advantage of time resolved interferometry is that it allows the researcher to investigate dynamic behavior of the material by looking at damage effects on wave propagation.[93] Dilatometry provides a quantitative means to explore interfacial damage due to oxidation, allowing thermal expansion experiments.[24] The strain introduced by thermal expansion mismatch plays a major role in TBC failure, so techniques for exploring thermal expansion are very important.

5. THEORETICAL PREDICTION OF INTERFACE STABILITY

Theoretical methods offer the opportunity to explore structure-property relationships in ideal metal-ceramic interfaces. Ultimately, improved understanding of the causal sequence leading to a particular interface structure and set of properties would enable further optimization of manufacturing parameters. Atomistic modeling constitutes the perfect laboratory in this respect. Within the limits of the specific approximations used for interatomic interactions, physical properties may be resolved to arbitrary accuracy and competing effects may be separated.

Here we will be concerned mainly with the interface structural stability and electronic structure. One of the most important factors determining the interface stability is the interface cohesive strength. Other factors may be equally important for stability of the interface, depending on the actual situation, e.g. corrosion resistance, thermal expansion and elastic matching of the metal and ceramic, the flexibility of the structure to release stress buildup during thermal cycling, stability towards structural degradation by unwanted interface segregation of certain elements and undesirable mixed phase formation at the interface. In this section, we give an overview of strategies by which theory can play an important role in helping characterize such interfaces. A recent and excellent review on the theoretical aspects of the M/C interface was given by Finnis[94] in 1996; we will therefore concentrate on later developments in the understanding of M/C interfaces.

6. ATOMISTIC APPROACHES

The discipline of atomistic modeling has proliferated tremendously over the past two decades, due to the increased capacity of modern computers. The basic trade-off in atomistic modeling is always between accuracy of

calculated energies and forces and, on the other hand, size of the atomic ensemble meant to model a macroscopic system. The larger the ensemble size, the smaller is the influence of miscellaneous finite size effects on the physical properties. However, the larger the system size, the more approximate the atomistic description necessarily becomes.

Which tradeoff to choose depends on the situation: some physical properties are insensitive to details in the interatomic potentials. In such cases, a model potential will provide essentially identical results to the exact, as long as the model potential reproduces certain characteristic quantities like, e.g., elastic constants and bulk cohesive energies.

Physical properties may be insensitive to details of the interatomic potential for a variety of reasons. For example at low temperatures, the atomic system may probe a bounded region of phase space, most often the elastic regime around the equilibrium state; and in this bounded region, the interatomic interactions may be represented well by a suitable model potential. Some classes of physical properties, like critical phenomena, are intrinsically insensitive to many details in the interatomic potentials, as they are controlled by collective behavior. For other physical phenomena, like melting, effects of fine details in the interatomic potentials tend to average out.

However, in other situations, there will be a strong sensitivity to details in the interatomic potential. This is the case when the physics and chemistry is governed by rare events, like crossing activation barriers and the breaking and forming of chemical bonds. If the transition state is not well characterized and included carefully in the parameterization data base for the model potential, the activation barrier is very likely to be described erroneously by the model potential, leading to wrong transition rates. This is where *ab initio* methods are needed.

In the sections below, the particular aspects associated with atomistic modeling of M/C interfaces will be reviewed along with applicable recent work done in this field.

6.1. Structural Models for M/C Interfaces

Atomistic approaches need a structural model to represent the real system. In this section, we will briefly discuss the most common choices of structural models along with advantages and disadvantages, in order to enable readers unfamiliar with details to critically judge results presented in the literature. We will then discuss issues involved in choosing the structure of the interface which involves lattice stoichiometry and misfit. The most common structural models of M/C interfaces fall into two main classes: cluster and slab representations.

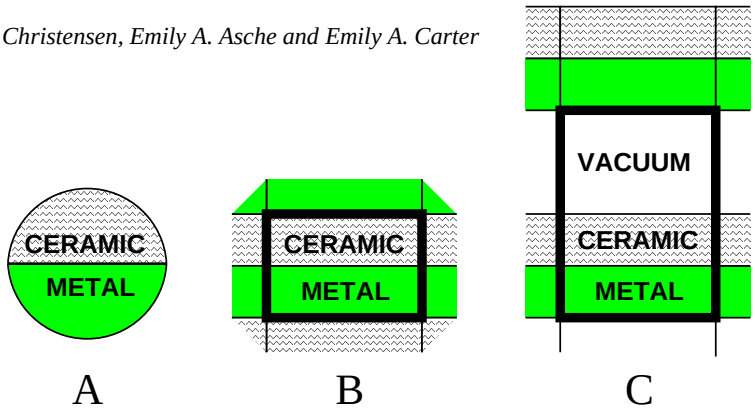

Figure 3 Schematic picture of M/C interface structural models.
A : Cluster model with vacuum around it.
B : Dense M/C interface unit cell, physically corresponding to a superlattice or sandwich structure.
C : Slab model with vacuum between periodic images perpendicular to the interface. Physically, the structure corresponds to M/C thin films. The borders of the periodically replicated unit cells in B and C are shown with bold lines.

6.1.1. Cluster Models These models are usually constructed by scooping out a small representative region (see Fig.3A) containing 5-30 atoms from the real M/C interface. Cluster models emphasize chemistry as local by only considering a small "active" region. Unfortunately, some early cluster studies used unrealistically small clusters, which were poor representations of the real interface they attempted to model.[95] In such cases, important long-range effects are missed.

Sometimes the ceramic side of the cluster is embedded in an array of the nominal anion and cation point charges in the proper structure, to emulate the real Madelung potential in the ceramic - this definitely improves the realism of the cluster model.[96–100] A Green's function constructed from the perfect host crystal has also been used to embed a ceramic cluster.[101] An alternative to anion and cation point charges is embedding the cluster into an array of overlapping anion and cation pseudopotentials,[102,103] thus trying to capture some of the electron-electron interaction with the surrounding ceramic medium. A supplement to this is mechanical embedding of the cluster via force field interactions with the surrounding substrate lattice,[104] so-called molecular mechanics. The latter neglects the perturbations in interatomic force constants caused by metallic adsorption and is likely to be rather inaccurate in the case of reconstruction or extensive relaxations in the interface region.

Cluster models have other generic finite size effects. Interfaces are often geometrically frustrated: for all metal atoms, there is a preferred adsorption

site on the ceramic surface. When one metal atom occupies that site, the neighboring metal atom generally will not be able to occupy an equally favorable site, due to the lattice mismatch between metal and ceramic. This frustration effect is not modeled properly, if the metal side of the cluster is too small. Another finite size effect is that the electronic density of states oscillates significantly with the cluster size.[105] This is critical near the Fermi level, because such oscillations in the density of states available for bonding to the ceramic is likely to produce predictions that converge slowly with cluster size.[106] This effect may be countered by "state preparation"[105] or by embedding the metal cluster in a periodic metal slab.[107] Unfortunately, since many finite size effects converge slowly with the cluster size, unmanageably large clusters may be required if not embedded properly. Furthermore, charged clusters are often considered, due to the nonstoichiometry of the ceramic piece of the cluster. Otherwise, the anions and cations will not be in the proper charge state, corresponding to the overall neutral bulk ceramic. A back-of-the-envelope estimate suggests that the nonphysical polarization induced by charged fragments may substantially affect the chemical predictions. The one significant advantage of cluster models is that the power of *ab initio* quantum chemical methods can be applied and therefore systematically converged results independent of experiment can be obtained, albeit for a small piece of the macroscopic system. This will be discussed in more detail shortly.

6.1.2. Slab Models These models are the preferred geometry in electronic structure methods originating from solid state physics. Periodic boundary conditions are applied to a unit cell representing the M/C interface. Therefore, slab models are restricted to coherent interfaces, which means that periodicity parallel to the interface is present - this corresponds to a "locked in" interface structure. Of course, the periodicity may have a long repetition length, which may not be modeled properly in some periodic slab calculations. There are two types of slab cells: those that do not include a vacuum layer and those that do. Dense unit cells (Fig.3B) physically correspond to sandwich structures with two M/C interfaces per unit cell. From an energetic point of view, this geometry is rather restrictive, because it requires sufficient symmetry such that the interfaces are identical (in order for the interface energy to be uniquely defined). Unfortunately, this requirement often restricts transverse relaxation, because the symmetry "locks" the M/C interface. On the other hand, if symmetry is enforced, this unit cell has no net perpendicular dipole moment, so that unphysical electrostatic coupling between the interfaces is avoided. It is also necessary to make both the metal and ceramic layer thick enough so that the interfaces do not interact

via electronic structure perturbations or strain, in order to have such a model realistically portray a single M/C interface.

A more general interface geometry is shown in Fig.3C. Physically this corresponds to an infinite array of M/C thin film couples separated by vacuum. A salient point is that the vacuum layers should be thick enough that adjacent M/C slabs do not interact. Interaction is possible in two ways: either via electronic wavefunction overlap in the vacuum or via Coulombic multipoles. The former interaction is usually vanishing, if more than ~ 10 Å of vacuum is present. The latter interaction is rather long-ranged, but fortunately methods have been devised to electrostatically decouple the slabs.[108–110] Of course, it is required that both the metal and ceramic layers are thick enough that the interface and surfaces do not interact.

The slab geometry also suffers from other finite size effects. If the extent of the unit cell parallel to the interface is too small, artificial strain effects are introduced, because the metal and ceramic are forced to be coherent by the periodic boundary conditions. Of course, this may be eliminated by enlarging the unit cell, which unfortunately leads to very computer-intensive calculations, as is the case with the cluster models. However for the slab model, the oscillations in the electronic density of states are not as dramatic when varying the number of atoms as in the case with clusters. This is because the slab is infinite parallel to the interface. This implies the spectrum is continuous, and the metal slab does not have an artificial band gap, unlike the metal cluster.

The artificial requirement of the unit cell periodicity perpendicular to the interface may be avoided, if a Green's function technique is used. Such techniques have been used for metal-metal interfaces[111] with high symmetry, but no such calculations for M/C interfaces have been reported yet to our knowledge.

6.1.3. Interface Stoichiometry If no experimental evidence is available concerning the orientation of the metal and ceramic crystals with respect to each other for a coherent interface, one needs somehow to produce a reasonable guess as to how the parent crystals may match up at the interface. The possibilities are immense, especially if the ceramic has low symmetry: first one needs to consider which faces from each parent crystal will match up. Symmetry considerations are often helpful at this point. Free energy consideration might also be guiding: weakly interacting M/C pairs are likely to match up on their low energy surfaces. Strongly interacting M/C pairs are more likely to match up on their high energy surfaces, because these generally contain more unsaturated atoms ready for bonding. However, if a new reaction phase forms at the interface, the situation becomes more complicated. If the bonding mechanism is dominantly electrostatic, image

theory, which we return to later, predicts the most polar ceramic surface to bind most tightly to the metal, i.e., it has the largest work of separation W. However, this does not mean that polar interfaces are most stable from a thermodynamical point of view; the most stable M/C interface that can be formed between the pair M and C is the one with smallest free energy, i.e. smallest interface tension γ^{MC}:

$$\gamma^{MC} = \gamma^{M} + \gamma^{C} - W - \sum_{i} \mu_i \Delta N_i \qquad (1)$$

This is the Dupré relation, generalized to allow mass exchange, e.g., with the ambient gas or with the bulk, at chemical potentials μ_i. ΔN_i is the change in abundance of species i in the interface region on forming the interface, and γ^{M}, γ^{C} are surface tensions of bare metal and ceramic, respectively. Thus, because a polar surface is energetically very unfavorable (theoretically γ^{C} diverges for a perfect, infinite polar ceramic surface), it may not be favorable to form an interface with a polar ceramic termination, even though the interface binding is relatively strong. Another approach for guessing the ceramic termination at the interface is to estimate anion/cation/metal bond combinations from the appropriate bulk phases. But no foolproof rules can be formulated on how the ceramic is terminated at the M/C interface. Stoichiometry is a complicating aspect in this context, because it depends on the chemical potentials present; and the interface chemistry changes dramatically with stoichiometry, as we will discuss later.

6.1.4. Lattice Misfit Having settled on some metal and ceramic surfaces that we think will match, we must determine the relative orientation and translation of these surfaces with respect to each other. Certain directions in the metal and ceramic are likely to be aligned for a stable interface. There will often be multiple minima, corresponding to different lock-in possibilities for the coherent interface. Lastly, the size and shape of the interface unit cell needs to be determined, if we assume a coherent interface, which is implicit if periodic boundary conditions are applied. A realistic unit cell will of course correspond to low strain on both the metal and ceramic side.

This vast number of possibilities calls for a systematic procedure to identify a subset of the most likely interface matchings of the parent crystals. This subset will then be the starting point for atomistic modeling. The question about unit cell size and shape is relatively simple to address. Many related procedures based on linear elasticity theory and lattice strain estimates may be adopted. The basic situation is sketched in Fig. 4: an overlayer unit cell A needs to be matched together with a substrate unit cell B. Matching pairs of unit cells are, in general, multiples of primitive cells in the interface plane for the metal and ceramic, respectively.

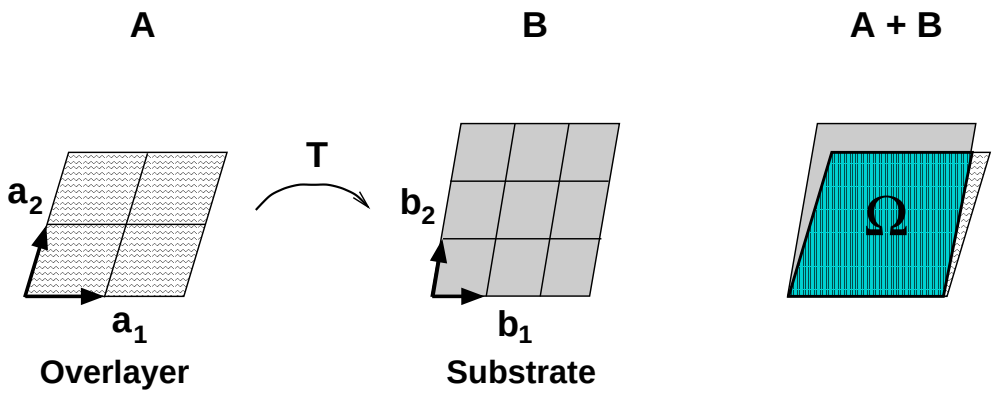

Figure 4 Schematic picture of M/C interface lattice matching.
A : Arbitrary overlayer unit cell constituted of many primitive cells spanned by the vectors a_1, a_2.
B : Arbitrary substrate unit cell constituted of many primitive cells spanned by the vectors b_1, b_2.
T : Linear transformation between A and B.
A+B : The "overlap" Ω between cells A and B.

The most crude approach to quantify the commensurability of the two given unit cells is to assign a mismatch factor based on the overlap between the cells A and B, i.e.

$$\mu = 1 - \frac{2|\Omega|}{|A| + |B|} \tag{2}$$

where $|A|, |B|$ and $|\Omega|$ signify the area of cell A, B and the overlap area, respectively. This quantity vanishes, if $A \equiv B$ and increases with decreasing overlap Ω, as sketched in Fig. 4. Thus one would like to choose an interface matching that minimizes μ.

Another geometrical approach was taken by Bolding and Carter,[112] who considered the matching of orthogonal unit cells. By taking multiples of each unit cell a suitable number of times in each direction, an arbitrarily low misfit might be achieved, in the same way that an arbitrary irrational number might be approximated by a rational number, if the numerator and denominator are sufficiently large. More specifically, they defined the strain variables

$$\delta_1^{nl} = \frac{la_1 - nb_1}{nb_1} \tag{3}$$

$$\delta_2^{mk} = \frac{ka_2 - mb_2}{mb_2}$$

where a_1, a_2, b_1, b_2 are the length of the basis vectors spanning the primitive unit cells of which A and B are multiples, see Fig. 4. (n, m, l, k) are integers giving the unit cell enlargement along each basis vector. Then Bolding and Carter proposed minimizing the quantity

$$\mu_{BC}^{nmlk} = w_1|\delta_1^{nl}| + w_2|\delta_2^{mk}| \tag{4}$$

which obviously is positive definite and vanishes at perfect coherency between A and B. Here w_1, w_2 are weight factors that might be related to the elastic properties of metal and ceramic. In Bolding and Carter's case, these weight factors were set to unity.

A more general approach would be to directly consider the elastic energy associated by deforming cell A into cell B so as to achieve coherency. If this deformation is designated by the 2×2 linear transformation matrix T

$$B = TA \tag{5}$$

where the matrices A and B contain the vectors spanning the (almost) matching pair of metal and ceramic unit cells, it is easy to show that the corresponding *exact* strain tensor ε and the corresponding elastic energy u is given by

$$\varepsilon = \frac{1}{2}[T^tT - I] \tag{6}$$

$$u = \frac{1}{2}\varepsilon : \gamma : \varepsilon \tag{7}$$

It is important to use the exact strain tensor definition, Eq. (6), to achieve rotational invariance with respect to lattice rotation; the conventional linear strain tensor only provides differential rotational invariance of u in Eq. (7).[113,114] A hierarchy of approximations may be used for the elastic tensor γ. The most rigorous approach is to transform the bulk elastic tensor c according to

$$\gamma_{pqrs} = R_{pi}^t R_{qj}^t c_{ijkl} R_{kr} R_{ls} \tag{8}$$

where a summation convention over same indices applies and R is the rotation matrix from interface to bulk crystal Cartesian frames.[113] However, it is not guaranteed that a thin film has the same ratio between elastic constants as the bulk crystal. Generally, six elastic constants are inequivalent in 2D elasticity theory, which follows from the permutational symmetry of c. As an approximation we may assume only c_{11}, c_{12} and c_{44} are nonvanishing, which is true for cubic symmetry. The lowest level of approximation is to

assume isotropy, in which case the relation $c_{11} = c_{12} + 2c_{44}$ applies and only a ratio, like c_{12}/c_{11}, needs to be estimated.

The approach assumes a fixed substrate; the most sophisticated procedure would be to minimize the elastic energy $u = u^{substrate} + u^{overlayer}$. This properly results in a small overall rescaling of the elastic energies. However, due to the physical simplicity of this elastic model, it is doubtful whether a better description is obtained unless both substrate and overlayer are highly anisotropic. Further, if material A is grown onto a bulk substrate B, it is unlikely that a transversal deformation of the substrate would take place in reality anyway.

It is instructive to compare this model to that of Bolding and Carter[112] discussed above, for the case where both substrate and overlayer have orthogonal lattices (in the interface plane). If we multiply the overlayer unit cell (l, k) times along a_1, a_2 and correspondingly the substrate unit cell (n, m) times along b_1, b_2, the transformation matrix T in Eq.(5) becomes

$$T^{nmlk} = \begin{pmatrix} \frac{nb_1}{la_1} & 0 \\ 0 & \frac{mb_2}{ka_2} \end{pmatrix} \tag{9}$$

Inserting this into the strain tensor Eq.(6), we get the harmonic energy, Eq.(7), to second order in the strain variables of Bolding and Carter,

$$u^{nmlk} = \frac{1}{2}\gamma_{11}(\delta_1^{nl})^2 + \frac{1}{2}\gamma_{22}(\delta_2^{mk})^2 + \gamma_{12}\delta_1^{nl}\delta_2^{mk} \tag{10}$$

Compared to the misfit factor of Bolding and Carter μ_{BC}^{nmlk}, Eq.(4), this expression contains a cross term and scales differently in the strain variables. Both expressions will be zero for perfect coherency $(\delta_1 = \delta_2 = 0)$, but for competing interface lock-in possibilities, one might expect Eq.(10) to be qualitatively more accurate. In conclusion, to find the most favorable unit cell lock-ins for a given substrate and overlayer lattice, from an elasticity point of view, we simply need to scan an expression like Eq.(10) in four indices (n, m, l, k) to find a subset of likely coherent interface unit cells. This is easily done on a computer.

In addition to the elastic energy, of course, the chemical interaction energy between metal and ceramic must be accounted for. The possibility of competition between elasticity and chemistry exists such that a rather elastically strained interface combination may be more stable than an unstrained one, because the strained one may have favorable chemical bonding between metal and ceramic atoms at the interface. Therefore, other interface combinations than the least strained need to be considered in general.

We now move on to discuss how one can assess structure and energetics of such interfaces from theory, starting from the most accurate models and ending with the most approximate.

6.2. *Ab Initio* Techniques

First principles techniques can be distinguished from semiempirical methods in that they include quantum mechanical effects explicitly using exact or moderate approximations for electronic exchange and correlation. Generally, explicit inclusion of quantum mechanical effects is computationally demanding, which restricts *ab initio* methods to small systems, typically less than 50 inequivalent atoms on modern workstations (1999). Using massively parallel computers, up to 300 inequivalent main group atoms can be handled *ab initio* today.[‡] In specialized cases, significantly more atoms can be handled by so-called $O(N)$ *ab initio* techniques, where the computational load scales essentially linearly with the number of atoms N. For insulating systems, tight binding calculations have shown that electronic density matrix methods[115–118] may be applied since the electronic density matrix has a finite range, and simulations with 650 atoms on a modern workstation have been reported.[119] Alternatively, divide and conquer[120] and localized wave function approaches[121–124] are well suited to achieve $O(N)$ scaling for insulating systems. If an artificial nonzero temperature is assumed for the electron system, density matrix[117,125–127] and localized wave function approaches[128] are also feasible for metallic systems, but imposing a nonphysical electronic temperature - unless it is removed by the end of the calculation[127] - is a dubious approximation for systems where the electronic density of states has much structure around the Fermi level, as in the case for transition metal/ceramic interfaces. For free-electron-like bulk systems, Orbital-free Density Functional Theory involving kinetic energy density functionals has allowed the treatment of ~6000 symmetry-inequivalent metal atoms.[129] The drawback of this method is that it is limited by the accuracy of the kinetic energy density functional, which is not known exactly for many-electron systems. Improving such functionals is, however, an active area of research.[130–144]

The restriction on the number of inequivalent atoms implies that only properties involving short length scales can be treated accurately, unless these properties are consistent with periodic boundary conditions. This restriction is rather severe in the case of a M/C interface, because the real interface is often transversely aperiodic and may contain long-ranged strain fields and defect structures perpendicular to the interface, which will require an extremely large unit cell to model. Thus only idealized M/C interfaces having small unit cells may be treated realistically by *ab initio* methods.

[‡]The definition of the concept *ab initio* is somewhat fluid, but usually means essentially free of empirical parameters. Being *ab initio* is generally considered a quality stamp, but one should be aware that some approaches, which are formally parameter-free, e.g. Thomas-Fermi density functional theory or *ab initio* tight binding, fail miserably outside limited application ranges.

This excludes many M/C combinations with large lattice mismatch between the metal and the ceramic, because a small interface unit cell implies that either the metal or the ceramic must be strained to an unphysical extent, leading to unphysical results induced by the artificial periodic boundary conditions. Still, for M/C interfaces where the natural lattice mismatch is low, *ab initio* studies of idealized M/C interfaces are instructive, giving valuable insights into quantum effects at the interface. We now discuss what has been accomplished with *ab initio* calculations of idealized interfaces.

6.2.1. Quantum Chemical Approaches A more precise description for this class is full wavefunction methods, where the basic variable is the full many-body wavefunction. The main problem with full wavefunction approaches is that the computational load increases drastically with the number of electrons N. At the Hartree-Fock level, the load increases as N^{3-4}, and the scaling with N increases steadily, the more complete the inclusion of electronic correlation. Since realistic modeling of interfaces requires quite large unit cells or large clusters, very few full wavefunction studies at and beyond the Hartree-Fock level have been reported in the literature. The interaction of a Cu[145] and a Pd[146] atom with a single MgO molecule have been studied using multireference configuration interaction. In both cases, binding of the metal to the O-atom in the MgO molecule was predicted as most stable (i.e. a linear molecule), with an "adsorption" energy of 2.28 eV and 2.65 eV for Cu and Pd, respectively. This is in accordance with the trend, observed by less accurate electronic structure methods, that metal atoms adsorb on top of the O atoms on the MgO(001) surface.

Hartree-Fock studies have been undertaken for cluster models of the Cu/MgO[147] and Ni/Al_2O_3[148] interfaces. Both studies find significant charge donation from the metal atom to the oxide conduction states. Hartree-Fock with *a posteori* electron correlation taken from a free electron gas (HF-CC)[154] in the supercell approach has been applied to Ag/α-Al_2O_3[155] and Ag/MgO(001).[155,156] Ag was found to be weakly bound to the completely O-terminated α-Al_2O_3(0001) surface, although significant charge transfer occurred. In agreement with density functional calculations, HF-CC calculations find Ag physisorbed above the O atoms in the MgO(001) surface. The adsorption energy above the O(Mg) site is 0.47(0.11) J/m^2, in good agreement with the experimental value, 0.45 J/m^2 for a thick Ag film.[157] However, this number is likely to be an average of adsorption of Ag over both O and Mg in separate domains, due to the (small) lattice misfit between Ag and MgO. A principal problem with the HF-CC method is that the *a posteori* free electron gas electronic correlation is not consistent with the exact exchange energy used in the underlying Hartree-Fock method - important error cancellations between exchange and correlation are lost.[158]

Initial tests[154] indicated a confidence level comparable to the best density functional models for exchange and correlation, but the approach needs to be tested on more systems to see if systematic errors exist. Related in spirit to the HF-CC method is the B3LYP[159] approach, which evaluates the electronic exchange-correlation energy as a weighted average of the exact exchange energy and the electron gas results for the exchange-correlation energy. The weighting parameters for this average were determined semiempirically, which makes this approach aesthetically unpleasant. However, for many molecules and finite clusters this approach has delivered accurate results. An instructive study has appeared,[160] which compares the adhesion of Cu atoms on MgO(001) using many electronic structure methods, ranging from various forms of density functional theory to post-Hartree-Fock approaches. Here, the results of the B3LYP method agreed rather well with the results obtained by the best post-Hartree-Fock approach, which estimated the binding energy of the Cu atom on MgO(001) to 0.40 ± 0.05 eV. This is probably the most accurate theoretical estimate of this quantity today. This paper also illustrated quite dramatically the sensitivity of the results to choice of DFT functional, which should sound a note of caution regarding the general applicability and transferability of current implementations of DFT.

In summary, full wavefunction methods are the most accurate *ab initio* methods, if electronic correlation is accounted for properly and the basis set for expansion of the electronic wavefunction is sufficiently complete – this might be difficult to judge by a non-expert. Furthermore, if a cluster model is used, it needs to be of sufficient size or be properly embedded for conclusions to be representative of an extended M/C interface.

6.2.2. Density Functional Theory For condensed phase systems, Density Functional Theory (DFT)[158, 161, 162] methods constitute the optimal compromise between accuracy and efficiency of all *ab initio* methods available today. The key point of DFT is to show that the exact quantum mechanical total energy E is a functional only of the total electron density $\rho(r)$, a 3-dimensional function, which corresponds to the intractable many-body electronic wavefunction Ψ, a $3N$-dimensional function where N is the number of electrons. The total energy within DFT, $E[\rho]$, is related to the total energy expressed in terms of Ψ, $E(\Psi)$, as

$$\begin{aligned} E[\Psi] &= <\Psi|\hat{T}^{elec} + \hat{U}|\Psi> + T^{ion} \\ &= T_s^{elec}[\rho] + U_{classical}[\rho] + U_{xc}[\rho] + T^{ion} \\ &= E[\rho] \end{aligned} \tag{11}$$

In principle, DFT is thus a formally exact mean field theory. Here T^{ion} is the ionic kinetic energy, $U_{classical}$ is the classical mean field Coulomb energy

for ionic cores and charge distribution ρ, T_s^{elec} represents the kinetic energy of the (noninteracting) electrons, and U_{xc} is a term describing lowering of electron-electron repulsion by correlated electronic motion and electronic exchange, as well as a kinetic energy component due to electron-electron interactions. U_{xc} in Eq. (11) is the only term whose functional form is not known exactly: the most commonly used approximations to it today are the Local Density Approximation (LDA) and the Generalized Gradient Approximation(s) (GGA).[149] A variety of slightly different GGA parameterizations have been proposed over the years;[150–153] indeed the choice of which GGA functional to use is a nonsystematic aspect of DFT calculations.

A slightly lower level of approximation than the LDA is the $X\alpha$ method, where the correlation energy is assumed to be proportional to the exchange energy, for which the LDA uniform electron gas expression is used. The $X\alpha$-approximation has been used for many pioneering metal/ceramic model studies. A consensus has developed in the literature[154, 160, 163–165] that the GGA on average is better than the LDA. But in certain cases, the GGA tends to overcorrect the LDA.[166, 167] For ionic surfaces, a significant lowering of the surface energy going from LDA to GGA has been noticed in some cases.[168] Another major drawback of the LDA/GGA approximations in this context is that they are not able to describe strongly correlated oxides, such as many 3d transition metal oxides.[169] These cases with breakdown of the LDA/GGA are due to two shortcomings of the LDA/GGA. The first is the general underestimation of the band gap, which can be traced back to a discontinuity feature in the exchange-correlation potential as function of electron filling[162] not captured by the LDA/GGA. The second is the self-interaction problem in the LDA/GGA in which electrons artificially interact with themselves due to the electron gas approximation for the exchange-correlation energy. This may be remedied by considering a self-interaction correction (SIC)[170, 171] scheme to the LDA/GGA, e.g. the LDA+U method.[172]

For insulating materials, such as ceramics, this normally does not pose problems, because the conduction band is empty and the band gap error is not reflected energetically. However, for M/C interfaces there may be some reason to worry, since mixing between oxide conduction bands and metal states will influence the magnitude of adhesion and charge transfer. These states may become filled, depending on the Fermi level on the metal side. Further research on this issue is warranted.

Because DFT-based techniques have the electronic density $\rho(r)$ as the basic variable, the computational load scales moderately with the number of electrons N, $O(N^{1-3})$. Thus they are able to handle significantly more atoms than traditional quantum chemical approaches that retain the full electronic many-body wavefunction as the basic variational quantity. This favorable

scaling currently makes DFT-based techniques most promising for *ab initio* studies of M/C interfaces, and therefore we will emphasize this group of methods in our review.

6.2.2.1. Applications of DFT to M/C Interfaces An increasing number of studies using self-consistent DFT-based techniques have been reported recently. The most popular M/C interface among theoreticians has been Ag/MgO(001), due to its small unit cell and small lattice mismatch of 3% and hence simple epitaxial character. Furthermore, this interface is well characterized experimentally. Generally, studies based on electronic structure methods agree that this interface is characterized by weak physical rather than strong chemical adhesion, with marginal charge transfer to Ag, and the O-site as most favorable adsorption site.[155,156,173–175] The MgO(001) surface is stoichiometric (i.e., there is an equal number of Mg and O ions on the surface) and O is nominally in the O^{2-} charge state. As also noted by Finnis,[94] it is interesting to observe the scattering in adhesion energies obtained by different basis set expansions. For Ag adsorbed on top of O(Mg), the Full-Potential Linear Muffin Tin Orbital (FP-LMTO) method gives 1.59(0.78) J/m^2 for 3 layers of Ag,[176] the Full-Potential Linear Augmented Plane Wave (FLAPW) method gives 0.53(0.53) J/m^2 for 1 Ag layer,[174] whereas a Gaussian-based Linear Combination of Atomic Orbitals representation gives 1.9(1.08) J/m^2 for 1 Ag layer.[177] All of these studies were performed within the LDA, which is notorious for its tendency towards overbinding.[158] This overbinding trend is followed for the Ag/MgO system, confirmed by comparing to the experimental value 0.45 J/m^2 for a thick Ag film.[157] Again, this value is likely to be an average of alternating domains with Ag adsorbed over O and Mg respectively, due to misfit dislocations induced by strain. The scatter in the theoretical results is not explained by the extent to which relaxations in the interface region were included; all authors relaxed the Ag-O distance, and none included full relaxations in the oxide. The FP-LMTO study[176] relaxed the oxide planes perpendicular to the surface, the FLAPW study kept the oxide frozen. The free MgO(001) surface termination displays a rumpling of the ions; however, our own DFT calculations,[178,179] which feature full relaxation, show that the Ag-film smooths the MgO(001) surface rumpling, so that the oxide layer nearest to the interface is flat. Furthermore, the oxide interlayer distances are as in bulk MgO to within 0.005 Å. Fig. 5 displays a repeated unit cell from our calculations of an Ag layer on top of a MgO(001) surface. Thus, in this particular case, the structural constraint in the FLAPW study did not affect the results. The large variations in theoretical predictions remains an unsatisfying aspect of these calculations.

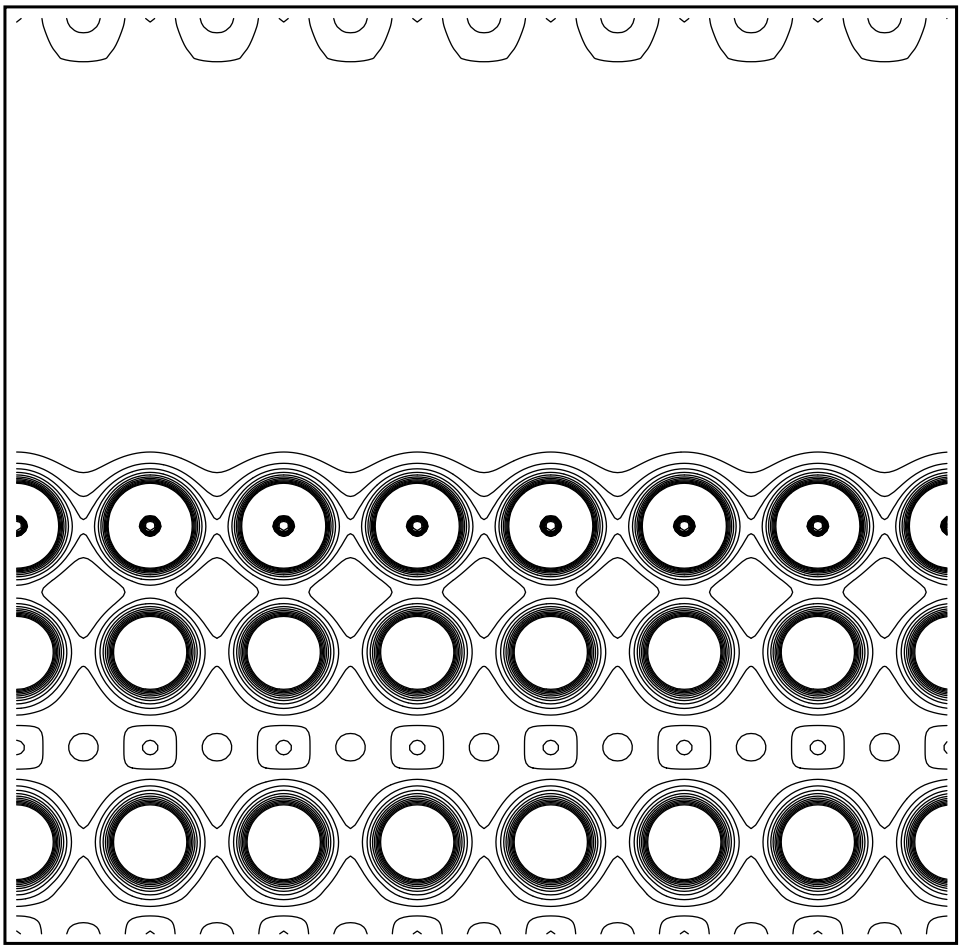

Figure 5 Ag/MgO(001) charge density plot cross-sectional view.
There are seven Ag sites on top of the layer of seven O sites. The Mg, with little valence charge, appear faintly beneath the O sites. Another O layer and Mg layer appears at the bottom. The contour lines at the top of the box are a result of periodic boundary conditions.

Polar M/C interfaces have only been studied sparsely. The polar (111) and nonpolar (100) Cu/MgO interfaces were compared in a slab calculation within the LDA.[180] As expected from the image model theory, the polar interface displayed a considerably higher work of separation. In addition these authors found a larger charge transfer and Cu-MgO orbital mixing for the polar interface.

Generally, *ab initio* methods have found that metals adsorb at the O-site of MgO(001) and that the Mg-site corresponds to a local maximum on the adsorption potential energy surface (PES), but the accord ends here. For Ag/MgO(001), Hong *et al.*[177] and Schönberger *et al.*[176] find a corrugation of the PES of the order of 50 % of the cohesive energy whereas Li *et al.*[174] find an extremely flat PES with corrugation less than 1 %. For comparison, for Pd/MgO(001), Goniakowski[181] finds a corrugation of order 20 %. Thus even though these systems appear easy to study, the disagreement upon even qualitative features of the interaction is rather disturbing.

It is an interesting question whether the GGA improves the agreement with experiments, as is often the case, or even changes trends predicted within the LDA. We investigated this by calculating the Ag/MgO(001) adhesion within both the LDA and GGA, using state-of-the-art ultrasoft pseudopotentials[178] in a converged planewave basis. For Ag adsorbed on top of O(Mg), we obtain adhesion energies of 0.62(0.27) J/m^2 within the LDA and 0.23(0.06) J/m^2 within the GGA. This indicates that the GGA overcorrects the LDA somewhat, compared to the experimental value of 0.45 J/m^2.[157] Also, a sensitivity on details of how the GGA functional is parameterized has been noticed.[160,182]

Only recently have other M/C interface studies appeared that tested the GGA in this context. Pacchioni and Rösch[183] studied Ni and Cu on MgO(001) in a cluster model. As might be expected, they found that Ni binds more strongly than Cu, due to the open d-shell of Ni. In both cases, the O-site is favored. They found a significant lowering of the adsorption energy for Cu when using the GGA, 0.65 J/m^2, compared to the value 2.54 J/m^2 obtained recently in a cluster calculation using the LDA.[184] Pacchioni and Rösch also noted that in these cases metal-metal bonds were stronger than metal-substrate bonds, thus predicting a 3D (cluster) growth mode as opposed to layer-by-layer growth (wetting). A more systematic study of transition metal adsorption on MgO(001) using GGA was presented by Yudanov *et al.*,[175] using a cluster model. Interestingly, they found no obvious correlation between cohesion and d-band filling as indicated by other studies. They found that single Cu, Ag, Au, Cr, and Mo atoms exhibited weak interface bonds, whereas Ni, Pd, Pt and W atoms formed strong bonds. For Ag/MgO, they obtained 0.36 J/m^2, similar to our findings for a coherent Ag monolayer.

Square-planar M_4 cluster adsorption for M = (Ni, Cu, Pd, Ag) on MgO(001) has been studied within the GGA.[185] Although here open shell transition metals adsorbed stronger, metal-metal and metal-oxide bond competition were found to be complex. An extensive study of Cu growth on MgO(001) was performed for clusters with 1-13 Cu atoms.[186] Here again, the authors found

the metal-metal bonds stronger than the metal-ceramic bonds, thus favoring a 3D (cluster) growth mode. Relatively weak cohesion for the Cu/MgO interface is also expected on the basis of the large lattice mismatch (13 %) between the metal and ceramic.

Electronic structure calculations of metal/Al_2O_3 interfaces were initiated by Johnson and Pepper.[187] They modeled this interface with a metal-AlO_6^{9-} cluster using the Xα-method, with the metal atom adsorbed in an O-triangle emulating a hollow site on a O^{2-}-terminated surface. This study concluded the bonding became weaker as the transition-metal adsorbate became more noble, which was explained in the conventional orbital mixing picture, where antibonding levels become filled in the right side of the transition series. This picture was essentially confirmed by later investigators. Most authors focus on the O-terminated $\alpha-Al_2O_3(0001)$ surface, which is nonstoichiometric, as the substrate for metallic growth. Under oxygen deficient conditions, however, it is not clear that the O-termination is appropriate for growth modeling. Grazing incidence X-ray scattering data indicate that the $\alpha-Al_2O_3(0001)$ is Al-terminated under ultrahigh vacuum (UHV).[188,189] Furthermore, DFT calculations predict that the charge-neutral O-terminated $\alpha-Al_2O_3(0001)$ has a significantly higher cleavage energy[190] than Al-terminated $\alpha-Al_2O_3(0001)$. Experimentally, when Ni was deposited on $\alpha-Al_2O_3$ in UHV, no Ni-O interaction was detected by XPS.[191] It is certainly reasonable to consider Ni-Al bonds, since NiAl is a very stable alloy. In any case, discussions about which Al_2O_3-substrate termination at the clean metal/Al_2O_3 interface is most relevant can be somewhat academic, since reaction phases, like spinels (MAl_2O_4),[192] are often formed at the interface. Our point of view is that most structural possibilities, at this stage, are interesting, since they help to furnish a general understanding of the electronic structure of the M/C interface under various conditions.

We have used DFT to study the Ni/Al_2O_3 interface. These calculations were performed within the planewave DFT code VASP using ultrasoft pseudopotentials.[178,193] Calculations with one and three layers of α-Al_2O_3 deposited onto the Ni(111) surface were performed. Both Al and O terminations of the α-$Al_2O_3(0001)$ surface were examined. Fig. 6 displays a repeated view of a unit cell with relaxed atomic coordinates for a Ni(111)/$Al_2O_3(0001)$ interface calculation. The lighter atoms in the top layer correspond to aluminum and the darker atoms are oxygen. In the Al-terminated α-$Al_2O_3(0001)$ surfaces, it appears that interfacial bonding between the alumina and Ni substrate decreases with increasing Al_2O_3 thickness. This effect may contribute to the increased spallation observed experimentally with the thickening of the TGO.

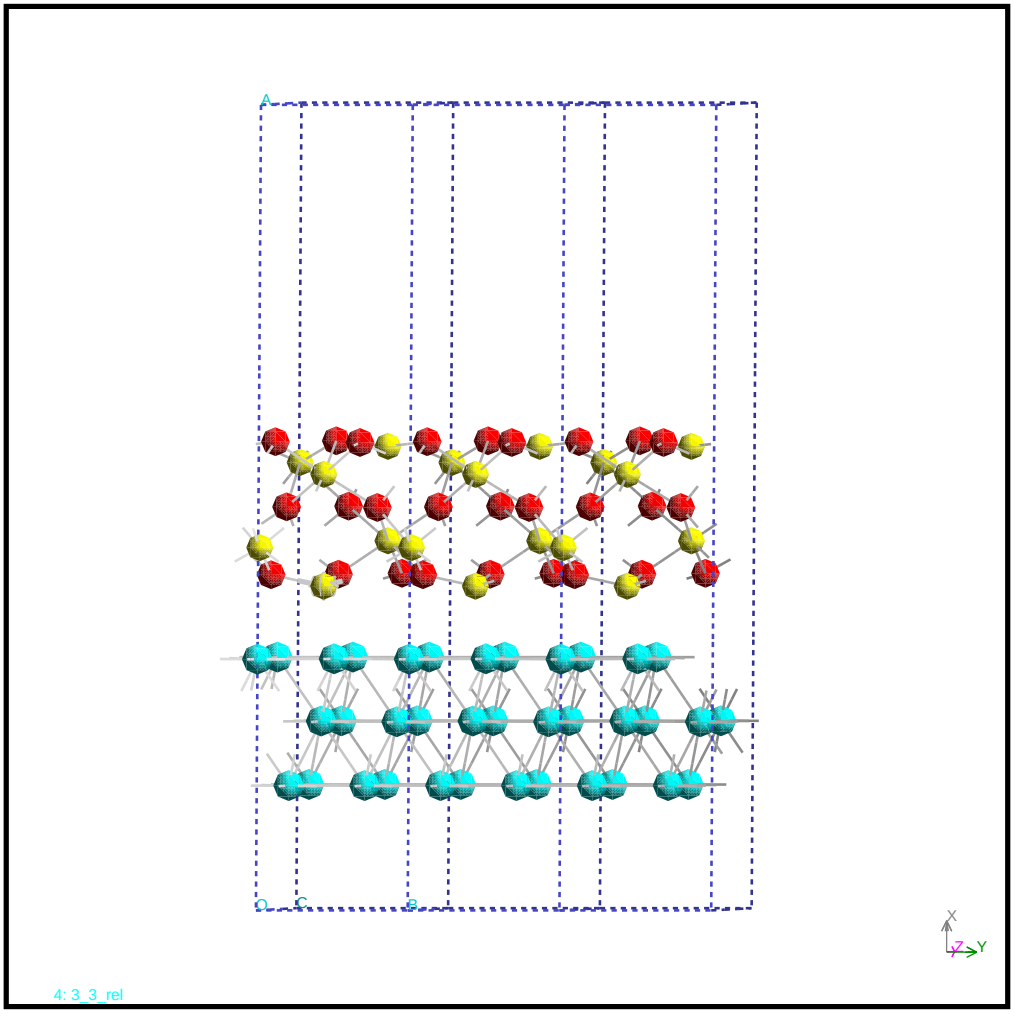

Figure 6 Ni(111)/Al_2O_3(0001) relaxed interface geometry

Kruse *et al.*[194,195] studied Nb monolayers (and multiple Nb layers to simulate bulk-like properties) on the O-terminated $\alpha-Al_2O_3$(0001) surface and found that Nb bonded to the hollow sites above the vacant octahedral sites. These authors emphasized the importance of ion relaxations when comparing competing adsorption geometries, a feature often lacking in many reported studies.

We have also undertaken studies of the Ni/ZrO_2 interface again using ultrasoft pseudopotentials within the VASP code.[178,196] Up to three layers of cubic ZrO_2(111) were "deposited" onto the Ni(111) substrate. As we found

for the Ni/Al_2O_3 interface, the work of separation (or adhesion strength) is quite large for the first monolayer; and, as more ZrO_2 is added, the intra-ceramic bonds increase in strength at the expense of the interfacial bonding. The adhesion strength is halved by the time that 3 layers of ZrO_2 are present. We find significant atomic distortions at the interface and a suppression of magnetism in the Ni layers nearest to the interface. The decrease in adhesion as ZrO_2 grows on Ni is consistent with the need for a bond coat alloy, since our predictions suggest thick ZrO_2 films may not readily adhere to the Ni-based superalloy under the TBC.

6.2.2.2. Aplications of DFT to Ceramics We have also studied bulk ZrO_2 in the monoclinic, tetragonal, and cubic phases as well as their associated low-index surfaces within the LDA to DFT.[48] We found that the most stable surfaces of tetragonal(t) and monoclinic(m) zirconia - the t(111) and m($\bar{1}$11) surfaces - are nearly degenerate in their surface energies. This provides an explanation for the preferential stabilization of t-ZrO_2 in small particles, where surface energies rather than bulk cohesive energies should determine the preferred structure. By using a Wulff construction[197] and known orientation relationships between the t and m phases, we showed that t(111) surfaces will transform to half m($\bar{1}$11) and half m(111) surfaces upon phase transformation. While the m($\bar{1}$11) surfaces are low in energy, the m(111) surfaces are predicted to have somewhat higher energies. Thus, we suggested that the suppression of the tetragonal to monoclinic phase transition in small particles may be due to the thermodynamically unfavorable nature of m(111) surfaces that would be forced to form. This idea prompted us to consider ways to keep ZrO_2 in the tetragonal phase over a very wide temperature range. One possible solution is to embed the small ZrO_2 particles in an alumina matrix, for example, as in the idea behind the nanolaminate films comprised of ZrO_2 and Al_2O_3 multilayers.

We then undertook a DFT-GGA study (within the Projector Augmented Wave formalism)[198] of the ZrO_2-Al_2O_3 interface, in order to understand how alumina might serve this purpose of confining/stabilizing small t-ZrO_2 particles and to shed light on the nature of the interaction between the bond coat and the TBC that occurs when the bond coat is oxidized to Al_2O_3.[199]

Our main conclusions are that the alumina/zirconia interface is weakly interacting: we find negligible charge transfer, no evidence of covalent bonding, and a very low adhesion energy of 1.065 J/m^2. The low adhesion energy is probably due to the fact that these surfaces of ZrO_2 and Al_2O_3 reconstruct to obtain approximate coordinative saturation, and therefore the lack of dangling bonds on these surfaces minimizes the interaction they have between them. This suggests that the role of the Al_2O_3 in the nanolaminate coatings is simply to act as a physical barrier to growth of the ZrO_2 layer and

that there is no true chemical bonding between these layers. Further, this weak interaction has broad implications for thermal barrier coatings. When the bond coat oxidizes, it is known that Al_2O_3 forms and that the lifetime of the TBC is tied to the oxidation kinetics of the bond coat. Therefore a possible microscopic explanation is now available: once Al_2O_3 forms, there is only a weak interaction between ZrO_2-Al_2O_3, and thus the ZrO_2 de-adheres at that point. A solution to this problem may be to minimize the amount of Al in the bond coat. Al may oxidize more readily than other elements present in the bond coat, and so perhaps increasing, for example, the amount of Cr in the bond coat may help inhibit spallation.

To summarize the application of DFT methods to M/C and ceramic interfaces, a significant "noise level" is apparent in predicted energetic features, originating from different basis set expansions, different degrees of ionic relaxation allowed for, and different approximations for electron exchange-correlation effects. However, qualitative trends from different studies are most often in agreement with each other and experiments. We now turn to a more approximate DFT technique which will allow larger systems to be studied.

6.3. The Harris Functional

A conceptually important approximation within DFT is the Harris functional.[200,201] In the Harris functional, the electronic ground state density ρ in Eq. (11) is approximated by a sum of overlapping atom-like densities ρ_m, suitably chosen[202,203] for each species $m = 1 \cdots M$

$$\tilde{\rho}(r) = \sum_{m=1}^{M} \sum_{i=1}^{N_m} \rho_m(r - R_{mi}) \tag{12}$$

where R_{mi} designates the position of the i^{th} atom of species m. This density ansatz makes it possible to express the cohesive energy and Hamiltonian matrix elements in terms of atomic contributions, which is very convenient for calculational and interpretive purposes. The Harris functional has been used as the starting point for deriving many approximate total energy schemes.[201,204–206] Inserting Eq. (12) into Eq. (11) we get

$$\tilde{E}[\tilde{\rho}] = \sum_{i \in occup} \varepsilon_i[v[\tilde{\rho}]] - \int v[\tilde{\rho}]\rho\, dr + U_{classical}[\tilde{\rho}] + U_{xc}[\tilde{\rho}] + T^{ion} \tag{13}$$

where the one-electron Schrödinger equations in the Kohn-Sham formalism[161] was used to get the first two terms and the one-electron potential v is given by

$$v[\tilde{\rho}] = \frac{\delta(U_{xc} + U_{classical})}{\delta\rho}|_{\rho = \tilde{\rho}} \tag{14}$$

The main problem with the Harris functional is that charge transfer and screening effects are not included properly, due to the static density ansatz, Eq. (12). This has led Finnis, on the basis of the image charge model[207,208] for M/C bonding, to object that the Harris functional - and therefore approximate total energy schemes derived from the Harris functional, such as non-self-consistent tight binding - are unsuitable for describing M/C bonding. He asserts that the attractive component of the M/C cohesion is mainly a polarization effect in the image charge model, which we will discuss later. However, despite the static density ansatz, Eq. (12), static screening effects are included via the eigenvalue sum in Eq. (13). Thus it remains to be demonstrated on a broad range of M/C systems how well the Harris functional performs. Encouraging results have been reported for Ag/MgO and Al/MgO with and without C and S impurities.[177,209]

6.4. Tight Binding

Tight binding (TB) schemes[210,211] refer to a rather ill-demarcated group of electronic structure techniques for describing interatomic interactions. The key merit of TB methods, compared to lower levels of interatomic potentials, is that they include quantum effects explicitly, although at a fairly approximate level. Their simpler nature produces a large computational speed gain over *ab initio* methods. This enables approximate studies of electronic structure effects in extended systems such as TBC's. In the chemically-oriented literature, TB methods are associated with Extended Hückel Theory(EHT)[212,213] or variants like Atom Superposition and Electron Delocalization Molecular Orbital (ASED-MO) theory, which is EHT augmented by an inter-nuclear repulsion term.[214]

The archetype for the TB total energy expression, E^{TB}, for ionic coordinates $\{R_n\}$ is

$$E^{TB}\{R_n\} = \sum_{i \in occup} \varepsilon_i\{R_n\} + E_{rep}\{R_n\} \tag{15}$$

where E_{rep} is a repulsive term balancing the propensity to gain energy in the spectral sum by increasing orbital coupling. The electronic spectrum $\{\varepsilon_i\}$ is obtained by solving a matrix eigenvalue problem

$$|\mathbf{H} - SE| = \mathbf{0} \tag{16}$$

corresponding to an implicit or explicit atomic basis, usually chosen to be minimal, i.e. one s-orbital, three p-orbitals per main group atom and five d-orbitals per atom for transition metals. **H** and **S** are the Hamiltonian and overlap matrices corresponding to this basis. Comparing Eqs. (15) and (16) to Eq. (13), the inherent approximations of TB appear : (i) The overlap

matrix **S** is often set to the unit matrix, i.e. the atomic basis is assumed orthogonal (orthogonal TB) - this reduces accuracy. Proper inclusion of the overlap matrix **S** (non-orthogonal TB) increases transferability, but is computationally more demanding. (ii) The Hamiltonian and overlap matrices are often fitted to simple pairwise analytic forms from a limited data-set, instead of being appropriate matrix elements with respect to a given basis. This reduces accuracy. (iii) The repulsive term E_{rep} is usually represented by an isotropic pair-potential, summed over all atomic pairs. The counterpart for E_{rep} in Eq. (13) is nonlinear in the exchange-correlation terms, therefore accurate representation of E_{rep} requires environment dependent pair-potentials[215–217] or three-body corrections. (iv) Usually there is a lack of charge self-consistency (i.e., charge redistribution, which is neglected in the density ansatz, Eq. (12)). This is usually only done by adjusting the diagonal Hamiltonian matrix elements H_{ii}.[211,218] Charge transfer may induce long-ranged effects, i.e. they may create a Madelung potential or induce band-bending. The most modern TB schemes put emphasis on a more realistic and detailed inclusion of self-consistency effects.[206,219]

The accuracy to which these points are treated determines the transferability of the TB scheme. For low level TB schemes, at most only the qualitative trends should be trusted. A pitfall in this context is overly parameterized TB schemes, i.e. too many fitted input parameters - this strategy will tend to hide inherent limitations. In principle, carefully worked out TB schemes can achieve almost the accuracy of self-consistent LCAO-DFT[204,206] without use of empirical fitting parameters.

Many interesting TB studies have been performed on the energetics and electronic structure of M/C interfaces. Most TB studies have focused on transition metals deposited on $\alpha-$alumina. Alemany *et al.*[220] obtained band structures using TB in an extended Hückel framework to study a variety of crystalline alumina terminations, where O anions were in the O^{2-} charge state. They generally found attractive interactions between adsorbed 3d-transition metal atoms coordinating with Al^{3+} cations but repulsive interactions when coordinating with O^{2-} anions, where the repulsiveness increased with nobleness. They found only small steric effects in this pattern, which provides support for phenomenological approaches to quantifying interface cohesion. They attributed the transition metal-Al^{3+} attraction to mixing of the adsorbate d-states and the coordinatively unsaturated Al^{3+} dangling bond (empty sp-hybrid) surface states.

When O ions were in the O^{-} charge state, the anions were found to be very reactive, with maximum interface adhesion for V and decreasing monotonically towards each side in the d series, but with Cu anomalously stabilized. The interface strength of O^{-} terminated $\alpha-Al_2O_3(0001)$ is esti-

mated to twice that of the Al^{3+} terminated. This picture is in some qualitative disagreement with the findings of Nath and Anderson,[221] who found the interface bond strength to O^{-}-terminated $\alpha-Al_2O_3(0001)$ decreasing monotonically with nobleness along the entire transition series. The Nath and Anderson study used ASED-MO theory to investigate their semiempirical cluster models where bonding was composed of covalent, charge-transfer, and two-body repulsion terms. The uncertainty between different studies even at the qualitative level is a signature of the sensitivity on TB input parameters and specific approximations in the TB scheme applied. This is also seen comparing the results of Anderson *et al.*'s[222] ASED-MO cluster calculations to Ward *et al.*'s[223] approximate weighted H_{ij} extended Hückel slab calculations for Pt on α-$Al_2O_3(0001)$. Both authors agree that Pt binds to the O^{2-}-terminated surface by $\sim$ 0.1 eV/Pt, but for the Al^{3+}-terminated surface Ward *et al.*[223] find 3.7 eV/Pt whereas Anderson *et al.*[222] obtain 2.5 eV/Pt. Interestingly, in the same study, Ward *et al.* find that Rh does not bind at all whereas Pd does, opposite to the nobleness trend found for the O^{-} termination.

Ohuchi and Kohyama[191] conducted empirical TB energy-band (slab) calculations for many transition metal/alumina interfaces, where the α-$Al_2O_3(0001)$ was Al^{3+} terminated. They generally found the interface cohesion to change from ionic to covalent character, when moving from left to right in the transition series. They focused especially on Nb/α-$Al_2O_3(0001)$ interfaces, where they noticed that the electronic perturbation was essentially confined to the Nb-layer nearest to the Al_2O_3 surface. This observation is in contrast to the DFT study by Kruse *et al.*,[195] which found that the electronic perturbation of the Nb layers was significant away from the nearest layer. Although the Al_2O_3 in the study by Kruse *et al.* was O-terminated, this is more likely to be a consequence of truncation of the TB Hamiltonian to nearest-neighbor contributions and limited inclusion of self-consistency in the work of Ohuchi and Kohyama.

Impurities and dopants at the M/C interface are very important in TBC systems. This issue also has been addressed by TB studies. For the Ni/Al_2O_3 system, Hong *et al.*,[224] using clusters treated with ASED-MO theory, found S impurities significantly decrease the interface strength, due to S^{-2}-O^{-2} closed-shell repulsions increasing the distance of the Al^{3+} from the Ni surface layer. Anderson *et al.*[225] found increased interface adhesion for Y dopants at the Ni/Al_2O_3 interface. Open d-shell transition metals are indeed expected to have the greatest bonding to ceramics. Further, Ni and Y form rather stable alloys, suggesting favorable Ni-Y interaction at the interface. Application of dopants for TBC's of course requires the dopants to be stable at the interface upon thermal cycling.

The moral of the TB story is to judge the results with some caution, since as we outlined above, even predicted qualitative trends vary, depending on the parametrization and particular form of the TB scheme applied.

6.5. Semiempirical Potentials

Many issues important for the understanding and engineering of real life interfaces involve long length scales, such as static and dynamic macroscopic properties, interface defects, toughness, wear, corrosion resistance, complex reaction phases, phase transitions, and interface deadhesion processes. These aspects of interface modeling are far outside the reach of *ab initio* and TB methods described above, which currently - and for years to come - are limited to studying model systems mimicking authentic M/C interfaces.

Therefore, an important objective in the theory branch of M/C interface research is to envisage new types of interatomic potentials suitable for modeling M/C interfaces to bridge the length scale gap between theory and experiments. In this context, *ab initio* studies are very useful: first for exploring the qualitative nature of M/C chemistry which must by captured by novel model interaction potentials; secondly, to provide a broad database for testing new interaction potentials.

For metals and ceramics considered separately, reliable interaction potentials have been developed in the past. For many metals, embedded atom type potentials[226–230] have proven successful. Alternatives and refinements have been developed.[231–233] For ceramics, rigid-ion and shell model potentials[234] and their refinements[235–238] have proven equally capable.

For the M/C interface, atomistic interaction potentials have developed around the idea of the image charge interaction,[239] where the ceramic ions are attracted to their electrostatic images induced in the metal (assumed perfectly conducting). This simple picture gives the right order of magnitude for the cohesion. Image charge interaction is only accurate beyond the distance where wavefunctions of metal and ceramic overlap. In that case, the ceramic acts as an external Coulombic potential on the metal and Finnis[208] derived the image charge interaction from DFT for this case. At close range, where wavefunctions overlap, orbital mixing contributes to the M/C interaction. Finnis[208] argues that this may be represented by a closed-shell repulsion term by considering the ceramic as a perturbed noble gas crystal, where protons have been transferred from anions to cations but the electron distribution is kept frozen. This point of view may be valid for weak M/C interfaces, but needs corrections for strongly interacting M/C interfaces with significant charge transfer or covalent contributions to the bonding.

An interesting implication of the image interaction picture is that metals will generally adhere more strongly to polar rather than nonpolar surfaces. This is because the net-charged ceramic surface will induce a net-charged image in the metal. By contrast, polar ceramic surfaces themselves are unstable, also for electrostatic reasons.

A refinement of the image model, the discrete classical model (DCM), was also formulated by Finnis.[208] Here the perfectly conducting halfspace representing the metal is replaced by a halfspace of conducting spheres. This discretization of the metal is necessary for atomistic modeling; and further this refinement gives a more realistic short-range description than the image model, where the interaction energy diverges at the image plane (i.e., the metal surface). Unfortunately, Duffy *et al.*[240] found that the DCM predicts that Ag adsorbs over Mg^{+2} instead of O^{-2} on the MgO(001) surface,[240] at variance with all electronic structure calculations.

A hybrid model for full atomistic relaxation was used recently by Purton *et al.*[241] to simulate the weakly interacting Ag/MgO(001) interface. The metal was described by an embedded-atom potential, the ceramic by a shell model and the M/C interaction by the DCM (i.e. an atom interacts via 2 different potentials). These authors found that Ag adsorbed over O^{-2} and attributed this to the fact that they used a different short-range potential in the DCM than Duffy *et al.*[240] used.

This illustrates that we are far from the point where we can develop robust and transferable semiempirical potentials for the general M/C interface. This task is fundamentally difficult because the bonding changes character at the interface, from metallic to ionic, and because of the structural complexity present. This probably requires explicit inclusion of quantum effects, at least at a low level.

Because semiempirical potentials for M/C interfaces are not yet a mature field, simulation results that rely critically on details of the metal and ceramic layer adjacent to the interface need to be judged with great caution, because of the limited transferability expected for these potentials. For strongly coupled M/C interfaces, no reliable functional forms of atomistic interaction potentials have been proposed yet.

7. MULTISCALE MODELING

As mentioned before, a salient problem with the atomistic modeling of realistic M/C interfaces is the contemporary presence of effects on multiple length scales, chemical interactions in the interface region along with defect structures and strain fields extending far away from the interface region. Naturally, this is a well-recognized difficulty in many modeling applications, and numerous techniques have been introduced that attempt to overcome this

problem. One useful approach is to couple an active region (in our case the interface vicinity) which is treated explicitly atomistically, together with the surrounding system within linear elasticity theory.[242,243] Course-Grained Molecular Dynamics (CGMD) is also designed to allow the treatment of larger systems than would be accessible with conventional ab initio techniques.[244] In CGMD, a statistical course-graining method is used to derive the equations of motion from finite temperature Molecular-Dynamics(MD). Accordingly, these equations coincide with conventional MD for atomic-scale mesh sizes, which allows a smooth coupling of the length scales. As a result, CGMD provides a means to computationally concentrate on "active regions," by creating finer meshes there, while permitting large-system simulations.

Another promising approach is the quasicontinuum method proposed by Tadmor *et al.*,[245] which combines the finite element method with adaptive mesh techniques. Atoms are partitioned into "local" and "nonlocal" atoms, according to the strain at the atom. Atoms characterized by low strain (local atoms) are typically far from the active region, and the energy of these atoms is well-approximated by atoms in a perfect crystal subjected to a similar (low) strain. This energy can be obtained from standard first principles methods. Technically, the energy of the local atoms in the large, remote regions is obtained by finite element integration on a sparse grid. The nonlocal atoms are subjected to high strain in the vicinity of an active region. The cohesive energy of a "nonlocal" atom is calculated as an explicit function of its coordination shell in real space, out to a given cutoff radius, which is more time-consuming. Conventional atomistic simulations normally consider all atoms as "nonlocal", which is why the quasicontinuum method can treat of order 1000 times more atoms than feasible with conventional atomistic simulation.

A limitation of the present formulation is that it relies on the partitioning of the energy into atomic contributions, i.e.

$$E^{tot} = \sum_{i=1}^{All\ atoms} E_i \qquad (17)$$

where E_i is an average energy for a "representative" atom. This is a virtue of approximate schemes only, like the embedded atom method and pair-potentials; the exact total energy is a collective quantity and imposing energy separability, Eq. (17), for first principles methods introduces some degree of ambiguity, especially for the atoms treated as "nonlocal". Also due to the energy separability requirement, extension of the quasicontinuum method to multicomponent systems is less clear, if energies and forces are generated from *ab initio* methods. One may be able to get around this problem by

defining E_i in the sum in Eq.(17) to be the total energy per unit cell for an associated strained reference system.

No results for M/C interfaces using these rather new multiscale modeling techniques, even with approximate total energy schemes, have emerged yet to our knowledge; but studies of weakly coupled M/C interfaces using a hybrid potential, like that of Purton *et al.*,[241] would certainly be feasible.

In addition to bridging length scales, as in the quasicontinuum method, it is equally important to consider how to bridge time scales. For example, the time scale of atomic motion is many orders of magnitude smaller than the time scale for materials creep. One route to accomplish time scale bridging is the Kinetic Monte Carlo (KMC) technique.[246] In this method, the system is evolved stochastically according to probabilities given by ratios of rate constants k_i to k_{ref}, where k_{ref} is the fastest rate constant in the system. By first choosing randomly a species in the system and then choosing randomly from a palette of possible elementary events that may change the nature of that species, and comparing the rate constant ratio for the selected elementary event to a random number between 0 and 1, one has a prescription for how to evolve the system in a kinetic rather than an equilibrium manner. While this provides the means to get to long time scales, it does have one major drawback. One must specify in advance the allowed elementary processes; in so doing, one may actually constrain the behavior of the material under study. Further, deterministic dynamics have been sacrificed at the altar of stochastic behavior in order to gain the increase in time scales. However, first principles-derived KMC has been used successfully to study kinetic behavior for a number of different materials by our group[247] and others[248–252] (not all of which are listed here).

Recently, Voter proposed a method known as hyperdynamics, or hyper-MD, designed to accelerate molecular-dynamics simulations.[253,254] This acceleration is achieved by including a bias potential that raises the potential energy in the valley regions of the potential energy surface but leaves the potential in transition state regions unaffected. Because the bias potential does not affect transition state regions, even though the Transition State Theory (TST) escape rate is enhanced, the ratio of TST escape rates from a given state to adjacent states is preserved. As a result, the system should advance sequentially at an accelerated pace while preserving the relative probabilities of exact dynamics. Provided that the assumptions inherent in TST are obeyed for the processes of interest (i.e., no saddle point recrossings and no correlated events), this is an attractive method for reaching time scales orders of magnitude longer than those achieved by conventional molecular dynamics. Voter has also proposed a method to effectively parallelize MD

simulations.[255] This technique and the hyper-MD are beneficial in decreasing simulation time necessary for the observation of infrequent events.

Kinetic Monte Carlo and hyperdynamics methods have yet to be applied to processes involved in thermal barrier coating failure or even simpler model metal-ceramic or ceramic-ceramic interface degradation as a function of time. A hindrance to their application is lack of a clear consensus on how to describe the interatomic interactions by an analytic potential function. If instead, for lack of an analytic potential, one must resort to full-blown density functional theory to calculate the interatomic forces, this will become the bottleneck that will limit the size and complexity of systems one may examine, even with multiscale methods.

8. PHENOMENOLOGICAL APPROACHES

Phenomenological approaches has been very successful in some areas, e.g. Miedema theory[256] for predicting many quantities in metallurgy. The essential task in phenomenological theories is to identify a suitable set of physically meaningful variables, which are "linearly independent", to characterize the materials. Experimental data are then correlated against this set of variables and functional relations are fitted.

Li[257] explored such possibilities for M/C interfaces. He found that the interface cohesion correlated well with average metal electron density in bond regions, the free energy of formation, the band gap and the conductivity of the ceramic. This study mainly focused on transition metals, but the correlation with electron density seemed also to encompass simple metals and semiconductors as interface partners. Chatain *et al.*[258] stressed the local chemical aspect by correlating interface cohesion with a linear combination of the solution enthalpy of the ceramic anion and cation, respectively, in the bulk metal, plus a van der Waals term. For simple M/C interfaces, Bordier and Noguera's model tight binding study[259] indicates that the Fermi level of the metal and the degree of ionicity of the ceramic should be important variables for correlating experimental data. Of course, the diversity of the approaches and variable sets above illustrates that there is no unique strategy for understanding M/C cohesion.

9. CONCLUSIONS AND OUTLOOK

Understanding the behavior of the interfaces and bulk materials involved in thermal barrier coating failure due to the extreme environment created in aircraft engines is still in its infancy. This is primarily because the system involves complex interfacial chemistry and the materials issues span large length and time scales. In this review, we have focused on the atomic level

characterization. Once that is specified, it will be imperative to draw links between the atomic and the microstructural scales in order to understand the materials failure mechanisms completely.

Ultimately, an important goal of the structural studies described above is to provide a foundation for experiment and theory to investigate the dynamic behavior of M/C interfaces, especially under conditions similar in severity to those found in the combustion region of a gas turbine engine. However, as mentioned above, theoretical dynamical studies of this type would be highly nontrivial and to date are nonexistent. In fact, constructing techniques to make these dynamical studies feasible constitutes an active area of our own research program. Why have such simulations not been performed? It is because of the - at best - murky understanding of M/C bonding. In other words, the lack of dynamics simulations on such systems is indicative of a much deeper, unanswered question; namely, what is the true nature of the interaction between metal atoms and the atoms present in a ceramic? It is a much more difficult and complex system to characterize than either a metal itself or an isolated ceramic, each of which can be described independently with much simpler models (e.g., glue or embedded-atom models for metals, ionic or shell models for ceramics, etc.). It is the interface interaction which eludes understanding to date. Thus, the emphasis in this review on static rather than dynamic properties of these materials points out that theorists are not yet in a position to examine these systems dynamically on the large length and time scales which may prove necessary to fully simulate thermal barrier coating failure.

That said, we can still glean some insight from the static investigations, enough to even make some tentative conclusions about how to improve TBC's. It is clear that the ideal coating should consist of a stress-tolerant ceramic and an oxidation-resistant bond coating with nearly the same coefficient of thermal expansion and elastic modulus as both the ceramic and the Ni-based superalloy. The cost savings that such an ideal coating would produce is nontrivial: it has been estimated at 10^7 gallons of fuel per year for a fleet of 250 airplanes.

Use of nanostructured pure ZrO_2 might help create such an ideal coating, as recent experiments have shown that one can stabilize the tetragonal phase of undoped ZrO_2 up to a critical grain radius of 6 nm.[49] We have provided an explanation for the special stability of t-ZrO_2 in nanocrystals, based on surface energy arguments. Thus, appropriately synthesized nanocrystals of ZrO_2 might allow the use of pure rather than doped zirconia, which would eliminate possible sources of materials failure due to dopant diffusion. Furthermore, use of t-ZrO_2 would provide the stress tolerance required via the transformation toughening mechanism observed for t-ZrO_2.[48]

It may be that the life expectancy of a TBC is even more sensitive to the bond coating composition than to the ceramic top coat composition.[260] Oxidation of the bond coating to Al_2O_3 may also be a significant source of TBC spallation. We suggest that reducing the amount of Al in the bond coat may be necessary to avoid spallation, based on our first principles calculations.

Based on the theoretical work done to date, it appears that rare earth or transition metals with open d- or f-shells (the less noble the better) show the greatest adhesion to ceramics, presumably because there can be a degree of covalent bonding at the interface. On the other hand, one wants to utilize transition metals that are either oxidation-resistant or form oxides that adhere strongly to ZrO_2. This may explain the presence of Y in the bond coating, since oxidation of the Y metal to Y_2O_3 will produce an oxide that forms solid solutions with ZrO_2, i.e. it is strongly interacting. It suggests that one should consider metals that form other cubic-based metal oxides, such as cerium, for addition to the bond coat.

As one can see, exploring the atomic-level properties of thermal barrier coatings involves a complex set of issues. We have attempted to provide some background on methods available for preparing and characterizing TBC's experimentally, as well as presenting the hierarchy of theoretical methods available in computational materials science, including the trade-offs involved in the use of each one. It is our hope that a microscopic understanding, provided both by ever-improving theory and experiment, of the basic mechanisms for metal-ceramic adhesion, ion and metal atom diffusion, and ceramic phase transformations eventually will lead to substantive improvements in macroscopic properties of TBC's, resulting in extended survival in the extreme environment present in an aircraft engine.

Acknowledgment. This work was supported by the Air Force Office of Scientific Research.

References

[1] S.M. Meier, D.K. Gupta, and K.D. Sheffler, *J. Miner. Metals Mat. Soc.* **43**, 50 (1991).

[2] F.C. Toriz, A.B. Thakker, and A.K. Gupta, *Surf. Coat. Tech.* **39/40**, 161 (1989).

[3] D.J. Wortman, B.A. Nagaraj, and E.C. Duderstadt, *Mat. Sci. Eng.* **A121**, 433 (1989).

[4] F. Ernst, *Mat. Sci. Eng.* **R14**, 97 (1995).

[5] R. Brydson, H. Müllejans, J. Bruley, P.A. Trusty, X. Sun, J.A. Yeomans, and M. Rühle, *J. Microscopy* **177**, 369 (1995).

[6] S. Musikant, *What Every Engineer Should Know about Ceramics* (Marcel Dekker, New York, 1991).

[7] E. Ryshkewitch and D.W. Richerson, *Oxide Ceramics* (Academic Press, Orlando, 1985).

[8] R. Taylor, J.R. Brandon, and P. Morrell, *Surf. Coat. Tech.* **50**, 141 (1992).

[9] F.H. Stott, D.J. de Wet, and R. Taylor,*MRS Bull.* 46 (Oct. 1994).

[10] T.K. Gupta, J.H. Bectold, R.C. Kuznicki, L.H. Cadoff, and B.R. Rossing, *J. Mater. Sci.* **12**, 2421 (1977).

[11] A. Dominguez-Rodriguez and A.H. Heuer, in *Surfaces and Interfaces of Ceramic Materials,* Eds. L.C. Dufour *et al.* (Kluwer, 1989) pp.761-776.

[12] A.E. Hughes, in *Science of Ceramic Interfaces II*, Ed. J. Nowotny (Elsevier, Amsterdam, 1994).

[13] I. Nettleship and R. Stevens, *Int. J. High Tech. Ceram.* **6**, 1 (1987).

[14] T. Gupta, J. Bechtold and R. Kvznicki, *J. Mat. Sci.* **12**, 2421 (1977).

[15] R. Garvie, *J. Am. Ceram. Soc.* **20**, 23 (1984).

[16] J. Brandon and R. Taylor, *Surf. Coat. Technol.* **39-40**, 143 (1989).

[17] H. Frank, H. Brown and P. Duwez, *J. Am. Ceram. Soc.* **37**, 129 (1954).

[18] V. Pandolfelli, I. Nettleship and R. Stevens, *Proc. Br. Ceram. Soc.* **42**, 139 (1989).

[19] W. Pyda, R. Haberko and M. Bucko, *Ceram. Int.* **18**, 321 (1992).

[20] W. Pyda, R. Haberko and M. Bucko, in *Science and Technology of Zirconia V*, Ed. S. Badwal*et al.* (Technomic, PA, 1993).

[21] P. Diaz, M.J. Edirisinghe and B. Ralph, *Surf. Coat. Tech.* **82**, 284 (1996).

[22] P Diaz, M.J. Edirisinghe and B. Ralph, *J. Mat. Sci. Lett.* **13**, 1595 (1994).

[23] J.A. Haynes, E.D. Rigney, M.K. Ferber and W. D. Porter, *Surf. Coat. Tech.* **86-87**, 102 (1996).

[24] Dongming Zhu and R.A. Miller, in *Fundamental Aspects of High Temperature Corrosion*, Ed. D.A. Shores *et al* (Electronchemical Society Proceedings, Pennington, 1997), pp. 288-307.

[25] B.A. Pint, I.G. Wright, W.Y. Lee, Y.Zhang, K. Prüßner and K.B. Alexander, *Mat. Sci. Eng.* **A245**, 201 (1998).

[26] D.R. Clarke, R.J. Christensen and V. Tolpygo, *Surf. Coat. Tech.* **94-95**, 89 (1997).

[27] Kh.G. Schmitt-Thomas, H. Haindl and D. Fu, *Surf. Coat. Tech.* **94-95**, 149 (1997).

[28] P. Harmsworth and R. Stevens, *J. Mat. Sci.* **27**, 616 (1992).

[29] W.Y. Lee and D.P. Stinton, *J. Am. Ceram. Soc.* **79**, 3003 (1996).

[30] U. Leushake, T. Krell, U. Schulz, M. Peters, W.A. Kaysser and B.H.Rabin, *Surf. Coat. Tech.* **94-95**, 131 (1997).

[31] C.R. Aita, U.S. Patent 5.472.795 (1995).

[32] C.M. Scanlan, M. Gajdardziska-Josifovska and C.R. Aita, *Appl. Phys. Lett.* **64**, 3548 (1994).

[33] J. Yuan, V. Gupta and M. Kim, *Acta Metall. Mater.* **43**, 769 (1995).

[34] V. Gupta, J. Wu and A. N. Pronin, *J. Am. Ceram. Soc.* **80**, 3172 (1997).

[35] C. Funke, J.C. Mailand, B. Siebert, R. Vaßen and D. Stöver, *Surf. Coat. Tech.* **94-95**, 106 (1997).

[36] R.E. Taylor, K.D. Maglic, in *Compendium of Thermophysical Property Measurement Methods 1*, Ed. K.D. Maglic (Plenum Press, New York, 1984) p.336.

[37] R.E. Taylor, *Mat. Sci. Eng.* **A245**, 160 (1998).

[38] R.E. Taylor, in *Compendium of Thermophysical Property Measurement Methods 1*, Ed. K.D. Maglic (Plenum Press, New York, 1984), p.125

[39] S. Alaruri, L. Bianchini, A. Brewington, *Opt. Lasers Eng.* **30**, 77 (1998).

[40] B. Ealet, E. Gillet, V. Nehasil and P.J. Møller, *Surf. Sci.* **318**, 151 (1994).

[41] C.D. Qin and B. Derby, *J. Mat. Res.* **7**, 1480 (1992).

[42] C.D. Qin and B. Derby, *J. Mat. Sci.* **28**, 4366 (1993).

[43] T. Wagner, R. Kirchheim, and M. Rühle, *Acta Metall. Mater.* **43**, 1053 (1995).

[44] K.P. Trumble and M. Rühle, *Acta Metall. Mater.* **39**, 1915 (1991).

[45] N.L. Loh, Y.L. Wu, and K.A. Khor, *J. Mat. Proc. Tech.* **37**, 711 (1993).

[46] Q. Zhong and F.S. Ohuchi, *J. Vac. Sci. Tech.* **A8**, 2107 (1990).

[47] C.R. Aita, C.M. Scanlan, and M. Gajdardziska-Josifovska, *JOM* **46**, 40 (1994).

[48] A. Christensen, E.A. Carter, *Physical Review B* **58**, 8050 (1998).

[49] M.A. Shofield, C.R. Aita, P.M. Rice, and M. Gajdardziska-Josifovska, *Thin Solid Films* **326**, 106 (1998). *ibid.*, 117.

[50] M. Gajdardziska-Josifovska and C.R. Aita, *J. Appl. Phys.* **79**, 1316 (1996).

[51] G.M. Newaz, S.Q. Nusier and Z.A. Chaudhury, *J. Eng. Mater. Tech.* **120**, 149 (1998).

[52] A.G. Evans, G.B. Crumley and R.E. Demaray, *Oxid. Metals* **20**, 193 (1983).

[53] H.E. Evans and M.P. Taylor, *Surf. Coat Tech.* **94-95**, 27 (1997).

[54] H.E. Evans, *J. Mat. Sci. Eng.* **A120**, 139 (1989).

[55] Z. Suo, *J. Mech. Phys. Solids* **43**, 829 (1995).

[56] S.M. Meier and D.K. Gupta, *Trans. ASME* **23**, 245 (1993).

[57] T.S. Oh, R.M. Cannon and R.O. Ritchie, *J. Am. Ceram. Soc.* **70**, C352 (1987).

[58] I.E. Reimanis, B.J. Dalgleish and A.G. Evans, *Acta Mat.* **39**, 3133 (1991).

[59] J.D. Kuenzly and D.L. Douglass, *Oxid. Metals* **8**, 139 (1974).

[60] G.S.A.M. Theunissen, A.J.A.Winnubst and A.J. Burggraaf, in *Surfaces and Interfaces of Ceramic Materials,* Ed. L.C. Dufour *et al.*, (Kluwer, 1989) pp. 365-372.

[61] K. Schindler, D. Schmeisser, U. Vohrer, H.D. Wiemhöffer and W. Göpel, *Sensors and Actuators* **17**, 555 (1989).

[62] G.M. Ingo and G. Padeletti, *Surf Interface Anal.* **21**, 450 (1994).

[63] J. Daloe and D. Boone, "Failure Mechanisms of Coating Systems Applied to Advanced Turbine Engine Components", in *Proc. 42nd ASME Gas Turbine and Aeroeng. Congr.* (Orlando, 1997).

[64] B.A. Pint, A.J. Garrat-Reed and L.W. Hobbs, *Mater. High Temp.* **13**, 3 (1995).

[65] B.A. Pint, *Oxid. Metals* **45**, 1 (1996).

[66] B.A. Pint, A.J. Garratt-Reed and L.W. Hobbs, *J. Am. Ceram. Soc.* **81**, 305 (1997).

[67] B.A. Pint, *MRS Bull.* **19**, 26 (1994).

[68] P.Y. Hou, K. Prüßner, D.H. Fairbrother, J.G. Roberts, *et al., Scripta Materialia* **40**, 241 (1998).

[69] P.Y. Hou and J. Stringer, *Oxid. Metals* **38**, 323 (1992).

[70] H.J. Grabke, G. Kurbatov and H.J. Schmutzler, *Oxid. Metals* **43**, 97 (1995).

[71] K. Prüßner, E. Schumann and M. Rühle, in *Fundamental Aspects of High Temperature Corrosion VI,* Ed. D.A. Shores *et al.* (Electrochemical Society, Pennington, 1996), pp. 344-356.

[72] B.A. Pint, *Oxid. Metals* **48**, 303 (1997).

[73] W.P. Allen, N.S. Bornstein, in *High Temperature Coatings I*, Ed. N. Dahotre *et al.* (TMS, Warrendale, PA, 1995) pp. 193-202.

[74] G.H. Meier, F.S. Pettit and J.L. Smialek, *Mater. Corrosion* **46**, 232 (1995).

[75] M.A. Smith, W.E. Frazier and B.A. Pregger, *Mater. Sci. Eng.* **A203**, 388 (1995).

[76] J.C. Schaeffer, W.H. Murphy and J.L. Smialek, *Oxid. Metals* **43**, 1 (1995).

[77] J.G. Smeggil, A.W. Funkenbusch and N.S. Bornstein, *Metal Trans.* **17A**, 923 (1986).

[78] C. Sarioglu, J.R. Blachre, F.S. Pettit and G.H. Meier, in *Microscopy of Oxidation 3*, Eds. S.B. Newcomb and J.A. Little; Institute of Metals, London, United Kingdom (1997), pp. 41-50.

[79] R.J. Christensen, D.M. Lipkin and D.R. Clarke, *Appl. Phys. Lett.* **69**, 3754 (1996).

[80] T. Troczynski and J. Camire, *Eng. Fracture Mech.* **51**, 327 (1995).

[81] V. Gupta, A.S. Argon and J.A. Cornie, *J. Mater. Sci.* **24**, 41 (1989).

[82] A.G. Evans and B.J. Dalgleish, *Acta Metall. Mater.* **40**, S295 (1992).

[83] A.G. Evans, M. Rühle, B.J. Dagleigh and P.G. Charalambides, *Metall. Trans.* **21A**, 2419 (1990).

[84] M. Arai, T. Sakuma, T. Mizutani, K. Kishimoto and M. Saito, *J. Ceram. Soc. Japan* **106**, 198 (1998).

[85] J. Yuan and V. Gupta, *Acta Metall. Mater.* **43**, 781 (1995).

[86] A.S. Argon, J.A. Cornie, V. Gupta, L. Lev and D.M. Parks, *Mat. Sci. Eng.* **A273**, 224 (1997).

[87] V. Gupta, A.S. Argon, D.M. Parks and J.A. Cornie, *J. Mech. Phys. Solids* **40**, 141 (1992).

[88] J.N. Johnson, *J. Appl. Phys.* **52**, 2812 (1981).

[89] S. Eliezer, I. Gilath and T. Bar-Noy, *J. Appl. Phys.* **67**, 715 (1991).

[90] T.W. Conlon, *Contemp. Phys.* **26**, 521 (1985).

[91] M.F. Stroosnijder, in *Application of Particle and Laser Beams in Materials Technology*, Ed. P. Misaelides (1994).

[92] M.F. Stroosnijder and G. Macchi, *Nucl. Instrum. Meth. Phys. Res. B* **100**, 155 (1995).

[93] L. Tollier, R. Fabbro and E. Bartnicki, *J. Appl. Phys.* **83**, 1224 (1998).

[94] M. W. Finnis, *J. Phys.: Condens. Matter* **8**, 5811 (1996).

[95] V. E. Heinrich, *J. Cat.* **88**, 519 (1983).

[96] K.M. Neyman, S.Ph. Ruzankin, and N. Rösch, *Chem. Phys. Lett.* **246**, 546 (1995).

[97] X. Xu, H. Nakatsuji, M. Ehara, X. Lü, N.Q. Wang, Q.E. Zang, *Chem. Phys. Lett.* **292**, 282 (1998).

[98] F. Rittner, R. Fink, B. Boddenberg, V. Staemmler, *Phys. Rev. B* **57**, 4160 (1998).

[99] G. Pacchioni, A. M. Ferrari, A. M. Marquez, and F. Illas, *J. Comp. Chem.* **18**, 617 (1997).

[100] M. Fernandez-Garcia, J. C. Conesa, and F. Illas, *Surf. Sci.* **349**, 207 (1996).

[101] Y. Ferro, A. Allouche, F. Corà, C. Pisani, and C. Girardet, *Surf. Sci.* **325**, 139 (1995).

[102] D. E. Ellis, G. A. Benesh, and E. Byrom, *Phys. Rev. B* **16**, 3308 (1977).

[103] M.A. Nygren, L.G.M. Petterson, Z. Barandiaran, and L. Seijo, J. Chem. Phys., **100**, 2010 (1994).

[104] N. Lopez, G. Pacchioni, F. Maseras, and F. Illas, *Chem. Phys. Lett.* **294**, 611 (1998).

[105] P. E. M. Siegbahn and U. Wahlgren, *Int. J. Quant. Chem.* **42**, 1149 (1992).

[106] G. te Velde and E. J. Baerends, *Chem. Phys.* **177**, 399 (1993).

[107] N. Govind, Y. A. Wang, A. J. R. da Silva, and E. A. Carter, *Chem. Phys. Lett.* **295**, 129 (1998); N. Govind, Y. A. Wang, and E. A. Carter, *J. Chem. Phys.* **110**, 7677 (1999).

[108] J. Neugebauer and M. Scheffler, *Phys. Rev. B* **46**, 16067 (1992).

[109] G. Makov and M. C. Payne, *Phys. Rev. B* **51**, 4014 (1995).

[110] P. E. Blöchl, *J. Chem. Phys.* **103**, 7422 (1995).

[111] H. L. Skriver and N. M. Rosengaard, *Phys. Rev. B* **43**, 9538 (1991).

[112] B. C. Bolding and E. A. Carter, *Mol. Simul.* **9**, 269 (1992).

[113] N.W. Ashcroft and N.D. Mermin, *Solid State Physics*,444, Saunders College, Philadelphia, 1976.

[114] L.D. Landau and E.M. Lifshitz, *Theory of Elasticity*, 3rd Edition, **7** (Butterworth-Heinenann Ltd., Oxford, 1995).

[115] M.S. Daw, *Phys. Rev. B* **47**, 10895 (1993).

[116] X.-P. Li, R. W. Nunes, and D. Vanderbilt, *Phys. Rev. B* **47**, 10891 (1993).

[117] R. Baer and M. Head-Gordon, *Phys. Rev. Lett.* **79**, 3962 (1997).

[118] K.R.Bates, A.D. Daniels, and G.E. Scuseria, *J. Chem. Phys.* **109**, 3308 (1998).

[119] D. Sanchez-Portal, P. Ordejon, E. Artacho, and J. M. Soler, *Int. J. Quant. Chem.* **65**, 453 (1997).

[120] W. Yang, *Phys. Rev. Lett.* **66**, 1438 (1991).

[121] G. Galli and M. Parrinello, *Phys. Rev. Lett.* **69**, 3547 (1992).

[122] F. Mauri, G. Galli, and R. Car, *Phys. Rev. B* **47**, 9973 (1993).

[123] P. Ordejon, D. A. Drabold, M. P. Grumbach, and R. M. Martin, *Phys. Rev. B* **48**, 14646 (1993).

[124] E.B. Stechel, A.R. Williams, and P.J. Feibelman, *Phys. Rev. B* **49**, 10088 (1994).

[125] R. Baer and M. Head-Gordon, *J. Chem. Phys.* **107**, 10003 (1997).

[126] R. Baer and M. Head-Gordon, *Phys. Rev. B* **58**, 15296 (1998).

[127] R. Baer and M. Head-Gordon, *J. Chem. Phys.* **109**, 10159 (1998).

[128] T. Zhu, W. Pan, and W. Yang, *Phys. Rev. B* **53**, 12713 (1996).

[129] S.C. Watson and P.A. Madden, PhysChemComm, **1**, 1 (1998).

[130] L.-W. Wang and M.P. Teter, *Phys. Rev. B* **45**, 13196 (1992).

[131] M. Pearson, E. Smargiassi, and P.A. Madden, *J. Phys.: Condens. Matter* **5**, 3321 (1993).

[132] F. Perrot, *J. Phys.: Condens. Matter* **6**, 431 (1994).

[133] E. Smargiassi and P.A. Madden, *Phys. Rev. B* **49**, 5220 (1994).

[134] M. Foley, E. Smargiassi, and P.A. Madden, *J. Phys.: Condens. Matter* **6**, 5231 (1994).

[135] E.Smargiassi and P.A. Madden, *Phys. Rev. B* **51**, 117 (1995).

[136] M. Foley and P.A. Madden, *Phys. Rev. B* **53**, 10589 (1996).

[137] B.J. Jesson, M. Foley, and P.A. Madden, *Phys. Rev. B* **55**, 4941 (1997).

[138] E. Chaćon, J.E. Alvarellos, and P. Tarazona, *Phys. Rev. B* **32**, 7868 (1985).

[139] P. García-González, J.E. Alvarellos, and E. Chaćon, *Phys. Rev. B* **53**, 9509 (1996).

[140] P. García-González, J.E. Alvarellos, and E. Chaćon, *Phys. Rev. A* **54**, 1897 (1996).

[141] P. García-González, J.E. Alvarellos, and E. Chaćon, *Phys. Rev. B* **57**, 4192 (1998).

[142] P. García-González, J.E. Alvarellos, and E. Chaćon, *Phys. Rev. B* **57**, 4857 (1998).

[143] Y.A. Wang, N. Govind, and E.A. Carter, unpublished.

[144] Y.A. Wang, N. Govind, and E.A. Carter, *Phys. Rev. B* **58**, 13465 (1998).

[145] N. Lopez and F. Illas, *J. Phys. Chem.* **100**, 16275 (1996).

[146] N. Lopez and F. Illas, *J. Chem. Phys.* **107**, 7345 (1997).

[147] N. C. Bacalis and A. B. Kunz, *Phys. Rev. B* **32**, 4857 (1985).

[148] A. D. Zdetsis and A. B. Kunz, *Phys. Rev. B* **32**, 6358 (1985).

[149] J. P. Perdew, *Phys. Rev. B* **33**, 8822 (1986); J. P. Perdew, *ibid.* **34**, 7406(E) (1986).

[150] A. D. Becke, *Phys. Rev. A* **38**, 3098 (1988).

[151] J. P. Perdew and Y. Wang, *Phys. Rev. B* **43** 13 244 (1992); J. P. Perdew, J. A. Chevary, S. H. Vosko, K. A. Jackson, M. R. Pederson, D. J. Singh, and C. Fiolhais, *ibid.* **46** 6671 (1992).

[152] J. P. Perdew, K. Burke, and M. Ernzerhof, *Phys. Rev. Lett.* **77**, 3865 (1997).

[153] B. Hammer, L.B. Hansen, J.K. Norskov, *Phys. Rev. B* **59**, 7413 (1999).

[154] M. Causá, A. Zupan, *Chem. Phys. Lett.* **220**, 145 (1994).

[155] Yu. F. Zhukovskii, M. Alfredsson, K. Hermansson, and E. A. Kotomin, *Nucl. Instrum. Meth. Phys. Res. B* **141**, 73 (1998).

[156] E. Heifets, E. A. Kotomin, and R. Orlando, *J. Phys.: Cond. Matt.* **8**, 6577 (1996).

[157] A. Trampert, F. Ernst, C. P. Flynn, H. F. Fischmeister, and M. Rúhle *Acta Metall. et Mater.* **40**, S227 (1992).

[158] R. G. Parr and W. Yang, *Density-Functional Theory of Atoms and Molecules*, (Oxford University Press, New York, 1989).

[159] A. D. Becke, *J. Chem. Phys.* **98**, 5648 (1993).

[160] N. Lopez, F. Illas, N. Rösch, and G. Pacchioni, *J. Chem. Phys.* **110**, 4873 (1999).

[161] P. Hohenberg and W. Kohn, *Phys. Rev.* **136** B864 (1964); W. Kohn and L. Sham, *Phys. Rev.* **140** A1133 (1965).

[162] R. O. Jones and O. Gunnarsson, *Rev. Mod. Phys.* **61**, 689 (1989).

[163] E. G. Moroni, G. Kresse, J. Hafner, and J. Furthmüller, *Phys. Rev. B* **56**, 15629 (1997).

[164] J.E. Jaffe, Z. Lin, and A.C. Hess, *Phys. Rev. B* **57**, 11834 (1998).

[165] P. Ziesche, S. Kurth, and J.P. Perdew, *Comput. Mat. Sci.* **11**, 122 (1998).

[166] Y. M. Juan and E. Kaxiras, *Phys. Rev. B* **48**, 14944 (1993).

[167] L. Vitos, A. V. Ruban, H. L. Skriver, and J. Kollar, *Surf. Sci.* **411**, 186 (1998).

[168] J. Goniakowski, J. M. Holender, L. N. Kantorovich, M. J. Gillan, and J. A. White, *Phys. Rev. B* **53**, 957 (1996).

[169] V. I. Anisimov, F. Aryasetiawan, and A. I. Lichtenstein, *J. Phys.: Cond. Matt.* **9**, 767 (1997).

[170] J. P. Perdew and A. Zunger, *Phys. Rev. B* **23**, 5048 (1981).

[171] D. Vogel, P. Kruger, and J. Pollmann, *Phys. Rev. B* **54**, 5495 (1996).

[172] V. I. Anisimov, J. Zaanen, and O. K. Andersen, *Phys. Rev. B* **44**, 943 (1991); V. I. Anisimov, I. V. Solovyev, M. A. Korotin, M. T. Czyzyk, and G. A. Sawatzky, *ibid* **48**, 16929 (1993); A. I. Lichtenstein, J. Zaanen, and V. I. Anisimov, *ibid* **52**, R5467 (1995).

[173] P. Blöchl, G. P. Das, H. F. Fischmeister, and U. Schönberger, in *Metal-Ceramic Interfaces* , Acta-Scripta Metallurgica Proceedings, Series **4**, Eds. M. Ruhle, A. G. Evans, M. F. Ashby, and J. P. Hirth, (Oxford ; New York, 1990), p.9; A. J. Freeman and C. Li, *ibid* p. 2.

[174] C. Li, R. Wu, A. J. Freeman, and C. L. Fu, *Phys. Rev. B* **48**, 8317 (1993).

[175] I. Yudanov, G. Pacchioni, K. Neyman, and N. Rösch, *J. Phys. Chem. B* **101**, 2786 (1997).

[176] U. Schönberger, O. K. Andersen, and M. Methfessel, *Acta Metall. Mater.* **40**, S1 (1992).

[177] T. Hong, J. R. Smith, and D. J. Srolovitz, *Acta Metall. Mater.* **43**, 2721 (1995).

[178] We used the plane-wave code VASP, which is described in G. Kresse and J. Hafner, *Phys. Rev. B* **47**, 558 (1993); *ibidem* **49**, 14 251 (1994); G. Kresse and J. Furthmüller, *Comput. Mat. Sci.* **6**, 15 (1996); G. Kresse and J. Furthmüller, *Phys. Rev. B* **55**, 11 169 (1996); ultrasoft pseudopotentials are described in G. Kresse and J. Hafner, *J. Phys.: Condens. Matter* **6**, 8245 (1994).

[179] In each case, a plane-wave cutoff at 340 eV was used, implying that absolute energies were converged to within 6 meV/atom. The ultrasoft pseudopotential augmentation charge cutoff was 554 eV. A k-point sampling density of 0.05 Å^{-1} was used and all LDA and GGA calculations respectively were performed in the same unit cells to optimize error cancellation. The GGA parameterization used is that of Perdew *et al.* [PW91= *Phys. Rev. B* **46**, 6671 (1991)] Ultrasoft pseudopotentials with outermost pseudization radii $r_c = 1.52, 1.01, 1.50$ Å were used for Mg, O, Ag, respectively. Separate pseudopotential sets were

generated for both LDA and GGA, i.e. the pseudization was consistent with the exchange-correlation functional applied in the interface calculation. For LDA and GGA, the cubic bulk equilibrium lattice constants for MgO are predicted to be a_0 = 4.126 Å and 4.224 Å, respectively, both in good agreement with the experimental value a_0 = 4.205 Å. Our MgO(001) slab and vacuum region were each 4 layers thick, and we considered only one monolayer of Ag. Corrections for interslab multipole interactions, although small, were added.

[180] R. Benedek, M. Minkoff, and L. H. Yang, *Phys. Rev. B* **54**, 7697 (1996).

[181] J. Goniakowski, *Phys. Rev. B* **57**, 1935 (1998).

[182] B. Hammer, L. B. Hansen and J. K. Nørskov, *Phys. Rev. B* **59**, 7413 (1999).

[183] G. Pacchioni and N. Rösch, *J. Chem. Phys.* **104**, 7329 (1996).

[184] Y. Li, D. C. Langreth, and M. R. Pederson, *Phys. Rev. B* **52**, 6067 (1995).

[185] A. V. Matveev, K. M. Neyman, G. Pacchioni, and N. Rösch, *Chem. Phys. Lett.* **299**, 603 (1999).

[186] V. Musolino, A. Selloni, and R. Car, *Surf. Sci.* **402-404**, 413 (1998).

[187] K. H. Johnson and S. V. Pepper, *J. Appl. Phys.* **53**, 6634 (1982).

[188] M. Gautier, G. Renaud, L.P. Van, and B. Villette, *J. Am. Ceram. Soc.* **77**, 323 (1994).

[189] P. Guenard, G. Renaud, A. Barbier, and M. Gautier-Soyer, *Surf. Rev. and Lett.* **5**, 321 (1998).

[190] J. Guo, D. E. Ellis, and D. J. Lam, *Phys. Rev. B* **45**, 13647 (1992).

[191] F. S. Ohuchi and M. Kohyama, *J. Am. Ceram. Soc.* **74**, 1163 (1991).

[192] J. A. Haynes, E. D. Rigney, M. K. Ferber, and W. D. Porter, *Surf. Coat. Tech.* **86-87**, 102 (1996).

[193] We found that the metal's electronic and geometric structures were well converged with respect to slab thickness for a three layer Ni(111) slab. Accordingly, we used a three layer Ni(111) slab with a hexagonal unit cell of 4.975 Å side lengths and periodic boundary conditions. This corresponded to a fully relaxed bulk Ni lattice constant. The top two

layers of the Ni and all of the Al_2O_3 layers were allowed to relax with no symmetry constraints. Over 10 Å of vacuum layer was included above the M/C layers and a 5x5x1 **k**-point sampling grid was used. The pseudization radii $r_c = 1.29$ Å for Ni, 1.40 Å for Al, and 1.01 Å for O were used. Fermi surface smearing of 0.10 eV was employed during the relaxation and the kinetic energy cutoff for the basis was 270 eV with a 554 eV cutoff used for the augmentation charge of the ultrasoft pseudopotential. Once we reached the equilibrium structure, a final point calculation was performed with the kinetic energy cutoff increased to 340 eV, and the tetrahedron method with Blöchl corrections [P.E. Blöchl, O. Jepsen, and O.K. Andersen, *Phys. Rev B* **49**, 16223 (1994)] was employed instead of Fermi smearing. The nonlinear core correction for exchange and correlation [S.G. Louie, S. Froyen, and M.L. Cohen, *Phys. Rev. B* **26**, 1738 (1982); W. Maysenhölder, S.G. Louie, and M.L. Cohen, *Phys. Rev. B* **31**, 1817 (1985)], was employed. These calculations included spin polarization and were performed at the GGA (PW91) level. Our calculated c/a lattice constant ratio for the hexagonal cell was 2.73 which is the same as that found by experiment [H. d'Amour, D. Schiferl, W. Denner, H. Schultz, W.B. Holzapfel, *J. Appl. Phys.* **49**, 4411 (1978)] Our orthorhombic cell's lattice constant agreed within one percent of experiment (5.19 Å to 5.14 Å respectively). The GGA Ni lattice constant, used for the M/C interface calculations, was 3.51 Å in close agreement with the experimental value of 3.52 Å.[113]

[194] C. Kruse, M. W. Finnis, V. Y. Milman, M. C. Payne, A. de Vita, and M. J. Gillan, *J. Am. Ceram. Soc.* **77**, 431 (1994).

[195] C. Kruse, M. W. Finnis, J. S. Lin, M. C. Payne, V. Y. Milman, A. de Vita, and M. J. Gillan, *Phil. Mag. Lett.* **73**, 377 (1996).

[196] We again used a three layer Ni(111) slab. We employed a hexagonal unit cell (6.5Åx6.5Å) with periodic boundary conditions. We fixed the unit cell at the fully relaxed bulk lattice constant of Ni. Again, we allowed only metal atom relaxations of the top two layers of Ni; the ceramic was allowed to relax fully. No symmetry constraints were imposed. We include 10 Å of vacuum above the M/C film couple. Only the valence 5s and 4d electrons are treated explicitly for Zr; a justification of this is given in our earlier work on ZrO_2.[48] The pseudization radii used were 1.01 for O, 1.62 for Zr, and 1.29 for Ni. Once again, the nonlinear core correction for exchange and correlation was used. Calculations were carried out spin-polarized at both the LDA and GGA levels. A **k**-point sampling density of 0.05 $Å^{-1}$ (a 3x3x1 grid) was

used. Fermi surface smearing by 0.30 eV was employed to enhance convergence. Kinetic energy cutoffs were 270 eV for the plane wave basis and 554 eV for the augmentation charge of the ultrasoft pseudopotential. Although dipole corrections were calculated for the final structure's total energy, the effect was small. The Ni lattice constant was the same as in the Ni/Al_2O_3 calculations and was used for the interface calculations. The cubic ZrO_2 lattice constant for GGA was 5.10 Å, which agrees with the experimental value extrapolated to T=0 [H. G. Scott, *J. Mater. Sci.* **10**, 1527 (1975)].

[197] W.A. Harrison, *Electronic Structure and the Properties of Solids*, (Dover Pub., Inc., New York, 1989) p 231.

[198] P.E. Blöchl, *Phys. Rev. B* **50**, 17953 (1994).

[199] We considered a large number of possible interface matchings for cells with surface areas up to 50 $Å^2$. The lowest lattice misfit of 4 percent for a reasonably sized cell was determined to involve the α-Al_2O_3(1-102) surface bonding to c-ZrO_2(001). This growth orientation is in fact the same as what has been observed experimentally for YSZ grown on the (1-102) plane of sapphire, [F. Konushi, T. Doi, H. Matsunaga, Y. Kakihara, M. Koba, K. Awane, and I. Nakamura in *Layered Structures and Epitaxy Symposium*, Ed. J.M. Gibson *et al.* (Materials Research Society, Pittsburgh, 1986) pp.259-64; X.D. Wu, R.E. Muenchausen, N.S. Nogar, A. Pique, R. Edwards, B. Wilkens, T.S. Ravi, D.M. Hwang, and C.Y. Chen, *Appl. Phys. Lett.* **58**, 304 (1991); and G. Garcia, J. Casado, J. Llibre, A. Figueras, S. Schamm, D. Dorignac, and Ch. Grigis in *Proc. 13th Int. Conf. Chem. Vapor Deposition*, Ed. T.M. Besmann *et al.* (Electrochemical Society, Pennington, 1996) pp. 699-705] so we are modeling a relevant interface. The alumina substrate was 9 Å thick, enough to emulate a bulk ceramic surface, both with regards to electronic structure and relaxation effects (based on our systematic studies of ZrO_2 and Al_2O_3). The ZrO_2 overlayer is also about 9 Å thick and we also include 10 Å of vacuum in between these thin film couples, which is usually enough to ensure negligible coupling between the thin film couples unless a large dipole is present at the interface. Apart from periodic boundary conditions on the unit cell, no symmetry or constraints were imposed on the electronic density and ionic motion. The interface unit cells (lattice constants and cell angles) were not relaxed, but fixed to the values derived from the fully relaxed bulk unit cell of sapphire. We then performed fully self-consistent ionic relaxation for this alumina/zirconia interface structure. These calculations included 4 **k**-points (for an equispaced grid) and

were performed at the GGA level [J.P. Perdew and A. Zunger, *Phys. Rev. B* **23**, 5048 (1981); and A.D. Becke, *J. Chem. Phys.* **96**, 2155 (1992)].

[200] J. Harris, *Phys. Rev. B* **31**, 1770 (1985).

[201] W. M. C. Foulkes and R. Haydock, *Phys. Rev. B* **39**, 12520 (1989).

[202] M. W. Finnis, *J. Phys.: Condens. Matter* **2**, 331 (1990).

[203] N. Chetty, K. W. Jacobsen, and J. K. Norskov, *J. Phys.: Condens. Matter* **3**, 5437 (1991).

[204] O. F. Sankey and D.J. Niklewski, *Phys. Rev. B* **40**, 3979 (1989).

[205] K. Stokbro, N. Chetty, K. W. Jacobsen, and J. K. Norskov, *Phys. Rev. B* **50**, 10727 (1994).

[206] A. P. Horsfield, *Phys. Rev. B* **56**, 6594 (1997).

[207] A. M. Stoneham, *Appl. Surf. Sci.* **14**, 249 (1983).

[208] M. W. Finnis, *Acta Metall. Mater.* **40**, S25 (1992).

[209] J. R. Smith, T. Hong and D. J. Srolovitz, *Phys. Rev. Lett.* **72**, 4021 (1994).

[210] W. A. Harrison, *Electronic Structure and Properties of Solids*, (Dover, New York, 1989).

[211] D. Pettifor, *Bonding and Structure of Molecules and Solids* (Oxford, New York, 1995).

[212] P. W. Atkins, *Phys. Chem.* (W. H. Freeman, New York, 1994).

[213] R. Hoffmann, *J. Chem. Phys.* **39**, 1397 (1963).

[214] A. B. Anderson, *J. Chem. Phys.* **60**, 2477 (1974); *ibid* **62**, 1187 (1975).

[215] N. Chetty, K. Stokbro, K. W. Jacobsen, and J. K. Norskov, *Phys. Rev. B* **46**, 3798 (1992).

[216] K. Stokbro, N. Chetty, K. W. Jacobsen, and J. K. Norskov, *J. Phys.: Condens. Matter* **6**, 5415 (1994).

[217] H. Haas, C. Z. Wang, M. Fähnle, C. Elsässer, and K. M. Ho, *Phys. Rev. B* **57**, 1461 (1998).

[218] S. Froyen, *Phys. Rev. B* **22**, 3119 (1980).

[219] M. Elstner, D. Porezag, G. Jungnickel, J. Elsner, M. Haugk, Th. Frauenheim, S. Suhai, and G. Seifert, *Phys. Rev. B* **58**, 7260 (1998).

[220] P. Alemany, R. S. Boorse, J. M. Burlitch, and R. Hoffmann, *J. Phys. Chem.* **97**, 8464 (1993).

[221] K. Nath and A. B. Anderson, *Phys. Rev. B* **39**, 1013 (1989).

[222] A. B. Anderson, C. Ravimohan, and S. P. Mehandru, *Surf. Sci.* **183**, 438 (1987).

[223] T. R. Ward, P. Alemany, and R. Hoffmann, *J. Phys. Chem.* **97**, 7691 (1993).

[224] S. Y. Hong, A. B. Anderson, and J. L. Smialek, *Surf. Sci.* **230**, 175 (1990).

[225] A. B. Anderson, S. P. Mehandru, and J. L. Smialek, *J. Electrochem. Soc.* **132**, 1695 (1985).

[226] M. S. Daw and M. I. Baskes, *Phys. Rev. Lett.* **50**, 1285 (1983).

[227] M. W. Finnis and J. E. Sinclair, *Phil. Mag. A* **50**, 45 (1984).

[228] F. Ercolessi, E. Tosatti, and M. Parrinello, *Phys. Rev. Lett.* **57**, 719 (1986).

[229] K. W. Jacobsen, J. K. Norskov, and M. J. Puska, *Phys. Rev. B* **35**, 7423 (1987).

[230] A. P. Sutton and J. Chen, *Phil. Mag. Lett.* **61**, 139 (1990).

[231] J. A. Moriaty, *Phys. Rev. B* **38**, 3199 (1988).

[232] A. E. Carlsson, *Phys. Rev. B* **44**, 6590 (1991).

[233] M. Aoki, *Phys. Rev. Lett.* **71**, 3842 (1993).

[234] B. G. Dick and A. W. Overhauser, *Phys. Rev.* **112**, 603 (1958).

[235] M. Wilson and P. A. Madden, *J. Phys.: Condens. Matter* **5**, 2687 (1993).

[236] M. Wilson, M. Exner, Y. -M. Huang, and M. W. Finnis, *Phys. Rev. B* **54**, R15683 (1996); M. Wilson, U. Schönberger, and M. W. Finnis, *ibid*, **54**, 9147 (1996).

[237] M. Wilson, P. A. Madden, N. C. Pyper, and J. H. Harding, *J. Chem. Phys.* **104**, 8068 (1996).

[238] A. J. Rowley, P. Jemmer, M. Wilson, and P. A. Madden, *J. Chem. Phys.* **108**, 10209 (1998).

[239] A. M. Stoneham and P. W. Tasker, *J. Phys. C: Solid State Physics* **18**, L543 (1985).

[240] D. M. Duffy, J. H. Harding, and A. M. Stoneham, *J. Appl. Phys.* **76**, 2791 (1994).

[241] J. Purton, S. C. Parker, and D. W. Bullett, *J. Phys.: Cond. Matt.* **9**, 5709 (1997).

[242] S. Kohlhoff, P. Gumbsch, and H. F. Fischmeister, *Phil. Mag. A* **64**, 851 (1991).

[243] R. Thomson, S. J. Zhou, A. E. Carlsson, and V.K. Tewary, *Phys. Rev. B* **46**, 10613 (1992).

[244] R.E. Rudd and J.Q. Broughton, *Phys. Rev. B* **58**, R5893 (1998).

[245] E. B. Tadmor, M. Ortiz, and R. Phillips, *Phil. Mag. A* **73**, 1529 (1996).

[246] K.A. Fichthorn and W.H. Weinberg, *J. Chem. Phys.* **95**, 1090 (1991).

[247] M.R. Radeke and E.A. Carter, *Phys. Rev. B* **55**, 4649 (1997).

[248] P. Ruggerone, A. Kley, and M. Scheffler, *Comments on Cond. Matt. Phys.* **18**, 261 (1998).

[249] J.G. LePage, M. Alouani, D.L. Dorsey, J.W. Wilkins, and others, *Phys. Rev. B* **58**, 1499 (1998).

[250] M. Neurock and E.W. Hansen, *Comp. Chem. Eng.* **22**, S1045 (1998).

[251] M. Jiang, Y.-J. Zhao, and P.-L. Cao, *Phys. Rev. B* **57**, 10054 (1998).

[252] M.J. Caturla, *Comp. Mat. Sci.* **12**, 319 (1998).

[253] A.F. Voter, *J. Chem. Phys.* **106**, 4665 (1997).

[254] A.F. Voter, *Phys. Rev. Lett.* **78**, 3907 (1997).

[255] A.F. Voter, *Phys. Rev. B* **57**, R13985 (1998).

[256] A. R. Miedema and R. Boom, *Z. Metallk.* **69**, 183 (1978); F. R. de Boer, R. Boom, W. C. M. Mattens, A. R. Miedema, and A. K. Nissen, *Cohesion in Metals: Transition Metal Alloys*, (North-Holland, Amsterdam, 1988).

[257] J.-G. Li, *J. Am. Ceram. Soc.* **75**, 3118 (1992).

[258] D. Chatain, I. Rivollet, and N. Eustathopoulos, *J. Chim. Phys. et de Physico-Chim. Biol.* **83**, 561 (1986).

[259] G. Bordier and C. Noguera, *Phys. Rev. B* **44**, 6361 (1991).

[260] S. Stecura, *Thin Solid Films* **182**, 121 (1989).